2017

Synthesis and Characterization of Cu(II)-Cu(I) Mixed Valence Complexes

Hansani T. Lekam Wasam Liyanage
Eastern Illinois University

This research is a product of the graduate program in Chemistry at Eastern Illinois University. Find out more about the program.

The Graduate School

EASTERN ILLINOIS UNIVERSITY

Thesis Maintenance and Reproduction Certificate

FOR: Graduate Candidates Completing Theses in Partial Fulfillment of the Degree
Graduate Faculty Advisors Directing the Theses

RE: Preservation, Reproduction, and Distribution of Thesis Research

Preserving, reproducing, and distributing thesis research is an important part of Booth Library's responsibility to provide access to scholarship. In order to further this goal, Booth Library makes all graduate theses completed as part of a degree program at Eastern Illinois University available for personal study, research, and other not-for-profit educational purposes. Under 17 U.S.C. § 108, the library may reproduce and distribute a copy without infringing on copyright; however, professional courtesy dictates that permission be requested from the author before doing so.

Your signatures affirm the following:

• The graduate candidate is the author of this thesis.

• The graduate candidate retains the copyright and intellectual property rights associated with the original research, creative activity, and intellectual or artistic content of the thesis.

• The graduate candidate certifies her/his compliance with federal copyright law (Title 17 of the U. S. Code) and her/his right to authorize reproduction and distribution of all copyrighted materials included in this thesis.

• The graduate candidate in consultation with the faculty advisor grants Booth Library the nonexclusive, perpetual right to make copies of the thesis freely and publicly available without restriction, by means of any current or successive technology, including but not limited to photocopying, microfilm, digitization, or internet.

• The graduate candidate acknowledges that by depositing her/his thesis with Booth Library, her/his work is available for viewing by the public and may be borrowed through the library's circulation and interlibrary loan departments, or accessed electronically. The graduate candidate acknowledges this policy by indicating in the following manner:

_____Yes, I wish to make accessible this thesis for viewing by the public

___✓___No, I wish to quarantine the thesis temporarily and have included the *Thesis Withholding Request Form*

• The graduate candidate waives the confidentiality provisions of the Family Educational Rights and Privacy Act (FERPA) (20 U. S. C. § 1232g; 34 CFR Part 99) with respect to the contents of the thesis and with respect to information concerning authorship of the thesis, including name and status as a student at Eastern Illinois University. I have conferred with my graduate faculty advisor. My signature below indicates that I have read and agree with the above statements, and hereby give my permission to allow Booth Library to reproduce and distribute my thesis. My adviser's signature indicates concurrence to reproduce and distribute the thesis.

Graduate Candidate Signature

Faculty Adviser Signature

Printed Name

Printed Name

Chemistry

12/15/2017

Graduate Degree Program

Date

Please submit in duplicate.

Synthesis and Characterization of

Cu(II)–Cu(I) Mixed Valence Complexes

(TITLE)

BY

Hansani T. Lekam Wasam Liyanage

THESIS

SUBMITTED IN PARTIAL FULFILLMENT OF THE REQUIREMENTS
FOR THE DEGREE OF

Master of Science in Chemistry

IN THE GRADUATE SCHOOL, EASTERN ILLINOIS UNIVERSITY
CHARLESTON, ILLINOIS

2017

YEAR

I HEREBY RECOMMEND THAT THIS THESIS BE ACCEPTED AS FULFILLING
THIS PART OF THE GRADUATE DEGREE CITED ABOVE

12/15/2017

| THESIS COMMITTEE CHAIR | DATE | DEPARTMENT/SCHOOL CHAIR OR CHAIR'S DESIGNEE | DATE |

12/15/17

12/15/17

| THESIS COMMITTEE MEMBER | DATE | THESIS COMMITTEE MEMBER | DATE |

12/15/17

| THESIS COMMITTEE MEMBER | DATE | THESIS COMMITTEE MEMBER | DATE |

Synthesis and Characterization of Cu(II)–Cu(I) Mixed Valence Complexes

L. W. L. HANSANI THEJANIKHALA

Abstract

Our study was focused on synthesis and characterization of new family of metal complexes that mimic the active site of copper containing enzymes. Our approach focused on preparing a series of metalloligands which vary systematically in structure and use them in combination with additional metallic centers to synthesize our desired complexes.

We synthesized a main ligand, which is named as $HL^Q 2Pz$, which contain a quinoline body, one amide bond and two pyrazolyl rings. We synthesized a copper complex by deprotonating $HL^Q 2Pz$ using KOH. The ligand coordinated to the copper(II) center through its quinoline nitrogen, two of the pyrazolyl nitrogen and deprotonated amide nitrogen. Acetonitrile, which was used to recrystallize the compound solvent, filled the fifth coordination site of the copper. The synthesis of metalloligands were done by replacing the acetonitrile with deprotonated acids such as bis(pyrazolyl)acetic acid and 1,3-bis(pyrazolyl)-2-butanoic acid which has additional coordination sites. These metalloligands were combined with additional metallic centers using metal salts such as $Cu(CH_3CN)_4PF_6$ and $(Ph_3P)_2CuNO_3$ as the final step. This gave Cu(II)-Cu(I) mixed valence complexes like the active sites of multicopper enzymes. All the above-mentioned ligands were characterized by ^{1}H-NMR and IR spectroscopies. All the complexes were characterized using X-ray crystallography and UV-Vis, IR spectroscopies.

Dedication

I dedicate this thesis to my loving mother, father and husband who have always supported me throughout this journey.

Acknowledgments

I would like to thank all the people who have supported me, not only during the research, but throughout my master's degree completion. I would like to express my gratitude to my supervisor Dr. Radu F. Semeniuc for his guidance, encouragement and support throughout my research. I would like to thank Dr. Kraig Wheeler for spending his time to solve the crystal structures presented in this thesis. I would also like to thank my thesis committee for their guidance and support for the completion of my thesis. I would like to thank Department of chemistry, Eastern Illinois university for academic and financial support. Finally, I would like to thank Petroleum Research Fund for providing partial financial support for my research.

Table of Contents

List of Tables

Introduction

Results and Discussion

List of Figures

Introduction

List of Schemes

I. Introduction

I.1. Biomimetic chemistry and catalysis

"Biomimetic synthesis" is a term that was first used by Sir Robert Robinson in 1917 to describe chemistry that is inspired by biological processes.[1] Biomimetic chemistry covers a wide array of topics that include the synthesis and study of artificial enzymes, the self-assembly of small molecules in a manner similar to that of biological self-assembly, and the study of biological precedents to direct the total synthesis of natural products. In the field of biomimetic chemistry, researchers attempt to utilize the key principles and concepts used in biological systems for developing new chemical reactions and processes.[2]

"Biomimetic catalysis" generally refers to chemical catalysis that mimics certain key features of enzymatic systems.[2] Polymetallic systems were expected to have greater oxidizing and reducing power, the neighboring metals were expected to "cooperate" in promoting reactions and electronic interactions between metals, which might lead to distinct physical properties. The proper design of polymetallic complexes provides a new reactivity pattern and physical properties that could not be achieved with similar monometallic complexes.[3]

Enzymes are macromolecules, which are known to catalyze more than 5,000 reactions in biological systems[4]. Most enzymes are proteins although few are catalytic RNA molecules known as ribosomes.[5] Although enzymes have large three-dimensional structure only a small portion of enzymes structure is directly involved in substrate binding and catalysis which is called the active site.[6] These active sites contain several metals such as copper, iron, cobalt etc. which has different oxidation numbers. Depending on the number of metals present, the active site of the enzymes classified as monometallic, bimetallic, trimetallic or polymetallic.

A distinctive class of enzymes are those containing copper ions in their structure, see Figure I.I for the active sites of such enzymes. There has been an increased interest in the study of these species due to their involvement in many biological processes such as electron transfer and oxidation of various organic

substrates[7,8]. These proteins are found typically in bacteria, plants, insects and mammals, and they have

four main functions: (i) metal ion uptake, storage, and transport, (ii) electron transfer, (iii) dioxygen uptake,

storage and transport, (iv) catalysis.[8,9]
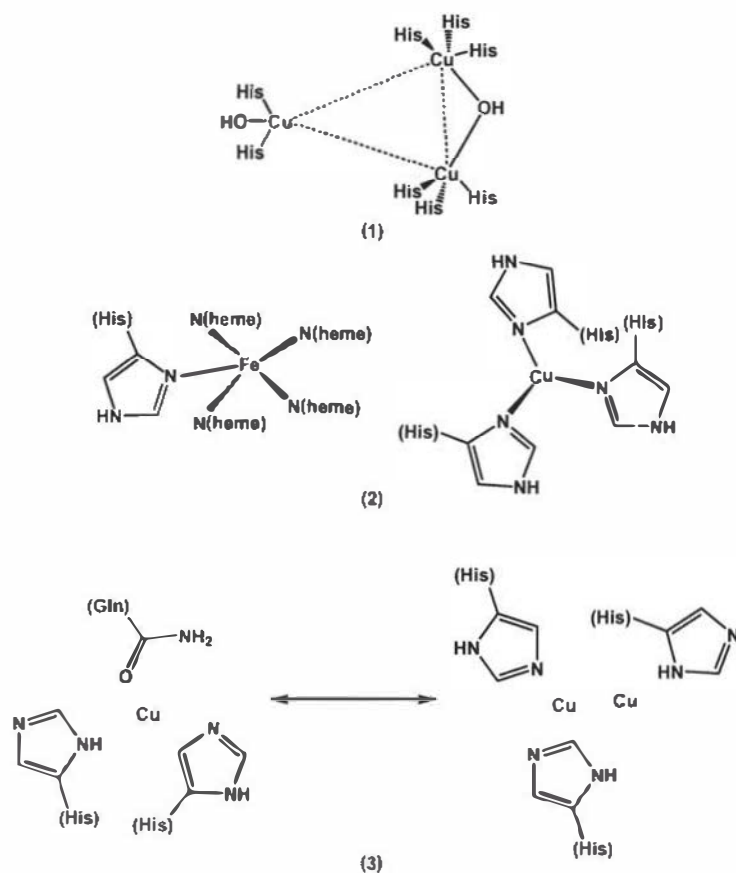
Figure I.1: Active sites of ascorbate oxidase (1), cytochrome c oxidase (2), methane monooxigenase (3).

Most of these enzymes are homonuclear with copper as the only metal and others are heteronuclear with

different types of metallic centers. These copper containing proteins were classified based upon their

spectroscopic properties, dividing them into three categories: type-1, type-2, and type-3. However, as more

structural data became available, these proteins were further divided into seven categories: type-1, type-2,

type-3, type-4 or multicopper, Cu_A, Cu_B, and Cuz clusters.[9,10] Some enzymes which contain copper centers

in their active sites are ascorbate oxidase, nitrite reductase, cytochrome c oxidase, methane monooxygenase

etc.

Some of the enzymes and oxygen transporters that contain a dinuclear copper site as active sites are nitrite reductase[11], haemocyanins (Hcs), catechol oxidases (COs) and tyrosinases (Tyr). These enzymes perform various functions. Hcs are the oxygen transporting proteins of molluscs and arthropods, COs catalyse the conversion of ortho-diphenols to ortho-quinones (catecholase activity) and Tys exhibit the same activity as COs but have a broader substrate range in the sense that they can also convert monophenols into ortho-quinones, presumably through an ortho-diphenol intermediate.[12]

Ascorbate oxidase contains a type 1 active site. These Type-1 copper protein active sites are known for their blue color originating from a strong absorption at 600 nm resultant of a Ligand to Metal Charge Transfer (LMCT) transition of a cysteine sulfur to the copper(II) ions.[11] Type-1 active sites are typically involved in electron transfer processes, multicopper oxidases, and redox enzymes. Active site of cytochrome c oxidase consists of a CuA type site and heme site which are arranged to efficiently funnel electrons to the catalytic heme/CuB center where O_2 reduction occurs.[13]

X-Ray crystallography was used to analyze the structure of the active site of nitrite reductase and ascorbate oxidase.[14] Nitrite reductase (NIR, see Figure I.2a) is an enzyme which reduces nitrate to nitric oxide, nitrous oxide etc. There are two classes of NIRs. A multi-haem enzyme reduces NO_2^- to a variety of products. Copper containing enzymes carry out a single electron transfer to produce nitric oxide.[15] Active site of nitrite reductase consists of two copper centers linked by a cysteine-histidine bridge. The distance between these two copper centers is about 12.5 Å. The active site of ascorbate oxidase (Figure I.2b) consists of three copper centers, which are linked by a bridge of branched cysteine, and two histidine rings in each protein, the cysteine ligated to the type-1 Cu is adjacent in the amino acid sequence to a histidine that ligates the partner Cu ion. This common bridging His-Cys unit is presumed to play an important role in facilitating electron transfer, particularly in view of the extensive unpaired electron spin delocalization onto the cysteine thiolate in oxidized type-1 centers.[14]
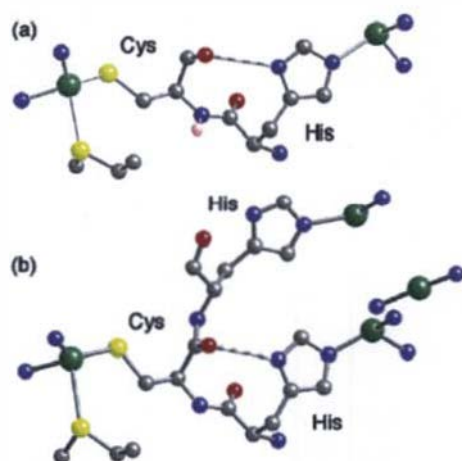
Figure I.2: Active site structures emphasizing the His-Cys bridge between two Cu centers of a) nitrite reductase (pdb 1AS7), b) ascorbate oxidase (pdb 1AOS). Figure from ref. 14. Color code: green = Cu, blue = N, red = O, yellow = S.

There were several investigations done by targeting to synthesize active sites of these copper containing enzymes. There was a research done to model the type-1 active site of copper containing enzymes. In this research they synthesized a LCuSCPh₃ (L = β-diketiminate shown in Scheme 1.1)[16] This complex was shown to accurately model the trigonal type I biosite structure, including the short and covalent Cu(II)-S(thiolate) bond[17] (see Figure I.3). Another research was done by targeting to synthesize "Cu-His-Cys-Cu"model complex. This was done by replacing one of the phenyl rings in the Ph₃CS⁻ ligand with a suitable N-donor group that would coordinate to a second metal center.[14]

Another attempt found in the literature was aimed to mimic the tricopper site of laccase.[18] In this study, Cu complexes of 2,2′-dipicolylamine (DPA) were prepared and tested as electrocatalysts for the oxygen reduction reaction (ORR). This was done to study the effect of multinuclearity on the ORR. In this study two Cu–DPA units were connected with a flexible linker, and a third metal-binding pocket was installed in the ligand framework. The ligands used as linkers in this research are shown in Figure I.4, and Figure I.5 show the crystal structures of those two complexes.

4
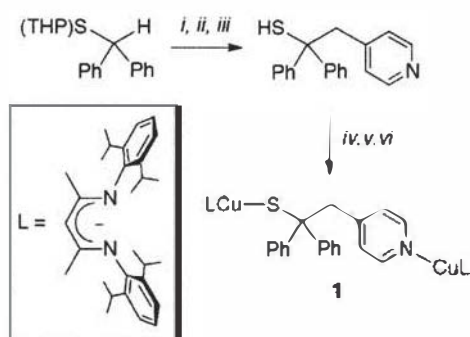
Scheme 1.1: Synthesis of "Cu-His-Cys-Cu using (THP)SC(H)Ph₂; Figure from ref. 14; Reagents: **(i)** BuLi, **(ii)** 0.5 ClCH₂PyHCl, **(iii)** NEt₃, HOCH₂CH₂SH, BF₃Et₂O, **(iv)** MeLi, **(v)** LCuCI, **(vi)** LCu(MeCN).
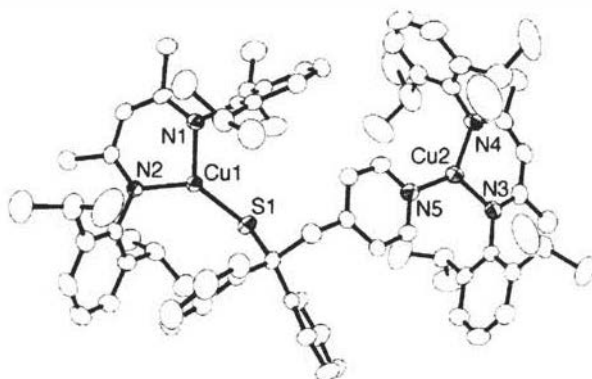
Figure 1.3: X-ray crystal structure of 1; Figure from ref. 14.
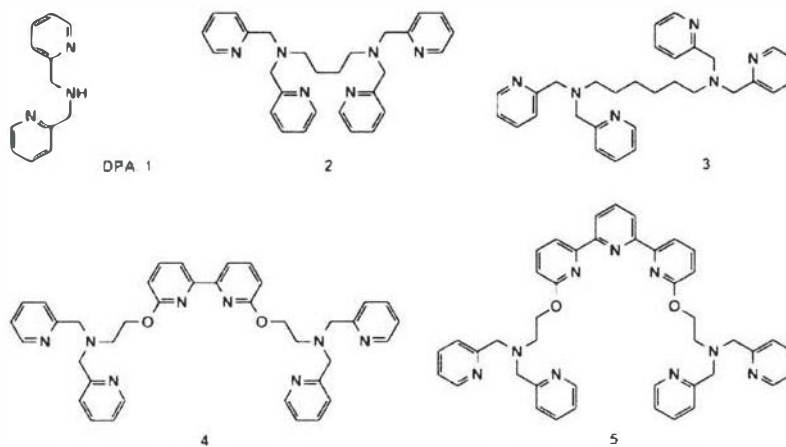
Figure 1.4: Ligands used in mimicking tricopper active site of laccase; Figure from ref. 18; 2,2'-dipicolylamine (DPA, **1**), *N*,*N*,*N'*,*N'*-tetra(pyridin-2-ylmethyl)butane-1,4-di-amine (**2**), *N*,*N*,*N'*,*N'*-tetra-(pyridin-2-ylmethyl)hexane-1,6-diamine (**3**), 2,2'-([2,2'-bipyridine]-6,6'-diylbis(oxy))bis(*N*,*N*-bis(pyridin-2-ylmethyl)ethan-amine) (**4**), and 2,2'-([2,2':6',2"-terpyridine]-6,6"-diylbis(oxy))bis(*N*,*N*-bis-(pyridin-2-ylmethyl)ethanamine) (**5**).
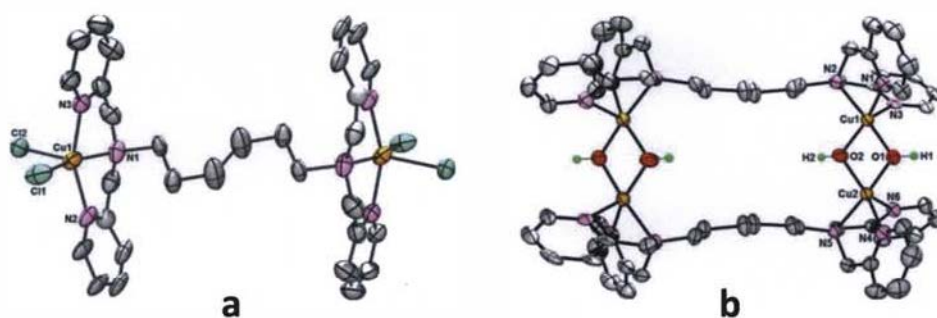
Figure I.5: Crystal structure of binuclear copper complex synthesized using linker 3 (see Figure I.4) before (a) and after (b) oxygenation; Figure from ref 18.

I.2. Ligands and metalloligands

A ligand is an ion or a molecule that binds to a metal atom through a functional group to form a coordination complex. The bonding with the metal generally involves formal donation of one or more of the ligand's electron pairs. The nature of metal–ligand bonding can range from covalent to ionic. Ligands can be classified in many ways such as based on denticity, field strength, or the number of metal atoms bound by one ligand.[19]

The coordination mode of the ligand is also important. Generally, the chelating mode of a ligand can be used to synthesize a simple complex and the bridging mode of a ligand can be used to synthesize a metalloligand.[20] Figure I.6 emphasize the difference between the chelating mode and the bridging mode of a ligand. For example, in Figure I.6 two ligands are depicted, 2,2'-bipyridine - which can be used to synthesize simple monometallic coordination complexes and 4,4'-bipyridine - which can be used to construct polymetallic complexes or extended architectures like metal-organic-frameworks (MOFs). However, chelating ligands with appended functional groups can also be used to synthesize metalloligands.

A metalloligand consists of a metal coordinated by a ligand system composed of two (or more) donor sets; one set is coordinated to the metallic center, which in turn directs the secondary donor site (or sites) to be suitably oriented for coordination to a second metal center (or centers). A metalloligand is also defined as the smallest building block that allows the construction of a more complex architecture, often a superstructure or the so-called supramolecular structure. From an application point of view, these

superstructures display new structural, chemical and properties that are unique and often depend on the resulting architecture, as pictured in Figure I.7.
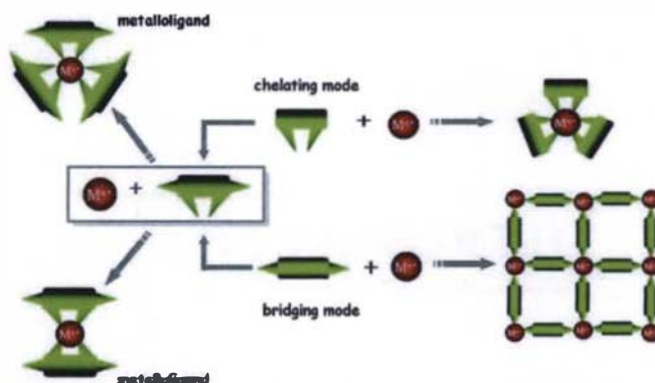
Figure I.6: Illustration of the Difference between the Chelating or Bridging Mode of a Ligand; Figure from ref. 20.
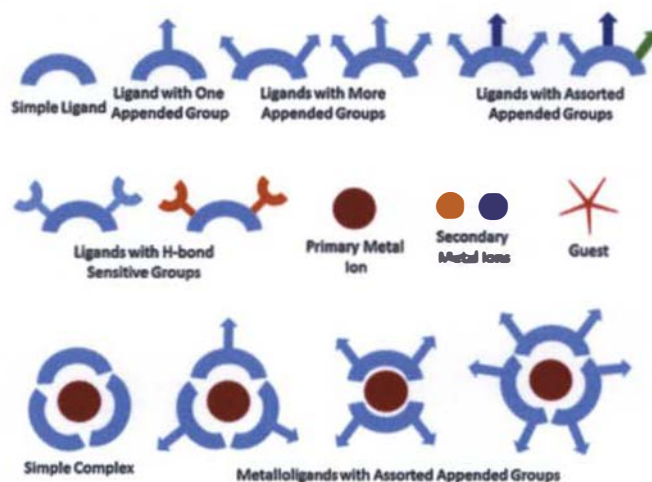
Figure I.7: Schematic representations of assorted ligands, metal ions, guest, complex, and metalloligands; Figure from ref. 21.

Since the "metalloligand" also contains a metal atom surrounded by some ligands as in a "simple coordination complex", it is essential to identify the difference between the two. In a simple complex, the metal ion is surrounded by ligands which are not offering appended functional groups. Even though a metalloligand also contains a metal atom surrounded by ligands, among those ligands, at least one contains an appended functional group which can be coordinated to a second metal atom. In other words, a

metalloligand is a species generated by a ligand having at least two donor sites. One of those sites binds to a primary metal ion and the other site coordinates with additional metal center(s).

Figure I.8 depicts a cartoon representation of a metalloligand. The dark blue rectangular site of this ligand is the primary binding site. The primary metal ion (the purple square) binds with this site. The light blue arrows depict the secondary coordination site, which can be used to coordinate to other metal ions. The example shown here has two secondary coordination sites. Depending on the orientation of the functional groups present in a metalloligand, the resulting architecture could be comprised of either discrete compounds or polymetallic species, either a 1-D chain, a 2-D sheet or 3-D structure.
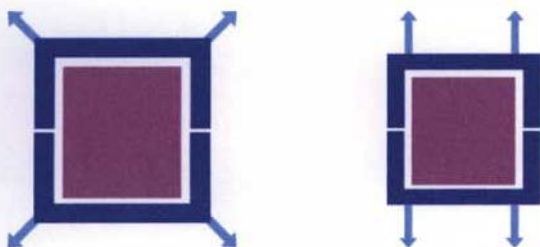
Figure I.8: Two metalloligands with appended functional groups pointed into two different directions

In the resulting architecture, the metal ion plays two essential functions: a structural task (direct and support the solid-state architecture), and a functional role (brings desired properties into the final complex). The propagation of a metalloligand into a higher-ordered structure can take place using metal-ligand covalent interactions or non-covalent interactions such as hydrogen bonds, π-π stacking and CH-π interactions between discrete species, as depicted in Figure I.9. This figure shows the self-assembly of some metalloligands into higher-ordered structures after coordination to a second metallic center. The metalloligand in Figure I.9a has a C_3 symmetry with three appended functional groups. As in the drawing, the geometrical orientation of these three appended functional groups will allow these metalloligands to coordinate with three different secondary metal atoms resulting a 2-D layer. Figure I.9b represents a similar coordination network with four appended functional groups, which can coordinate to four different metal atoms. The drawing in Figure I.9c represents a coordination network of a metalloligand having assorted functional groups with different chemical functionalities. These functional groups will show a preference

8

for certain types of secondary metal ions as described by the hard-soft acid-base theory. The drawing in Figure I.9d shows the interaction of a metalloligand with a guest molecule, which can be another metal complex, anion or a solvent molecule, while the drawing in Figure I.9e shows the self-assembly of metalloligand due to weak interactions such as hydrogen bonds. Hydrogen bond sensitive functional groups like carboxylic acids, phenols, amines, amides and halogens lead to these type of interactions as illustrated. The self-assembly due to the hydrogen bonding interaction follow a pattern similar to coordination bond driven self-assembly where the best hydrogen bond donor pairs with the best hydrogen bond acceptors and second best donor with the second best acceptor and so on.

Several donor groups can be used to build a metalloligand. Table I.1 lists various metalloligands, such as β-diketonate based metalloligands, acetylacetonate based metalloligands dipyrrin based metalloligands, mixed acetylacetonate–salen–dipyrrin based metalloligands, porphyrin based metalloligands, Schiff-base based metalloligands, pyridine/pyrazine-2-carboxylate based metalloligands, oxamide- and oxamate-based metalloligands, tris(triazolyl)borate based metalloligands, pyridine-amide based metalloligands, and dipyridyl-based metalloligands etc[21].
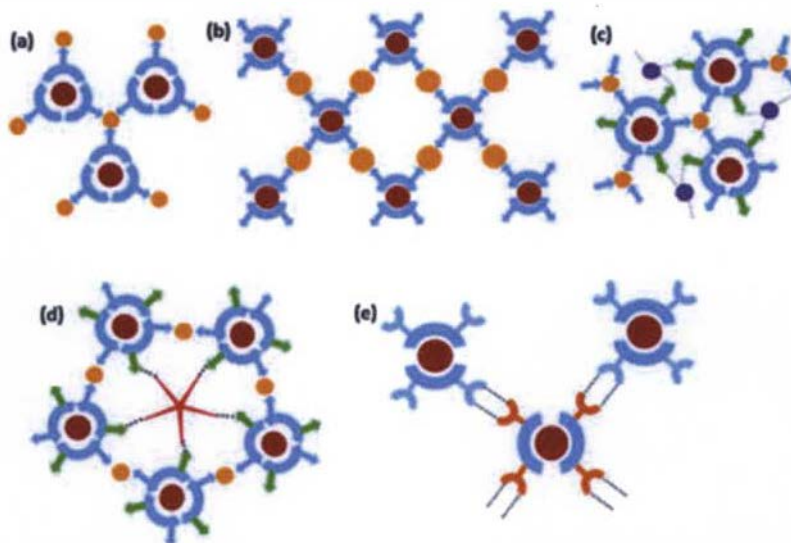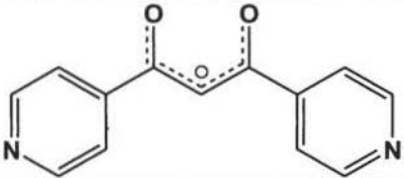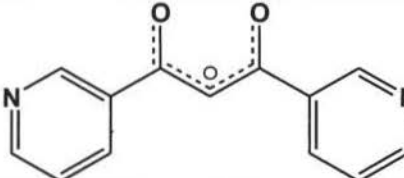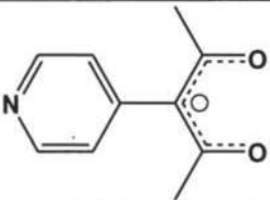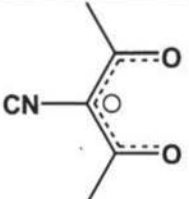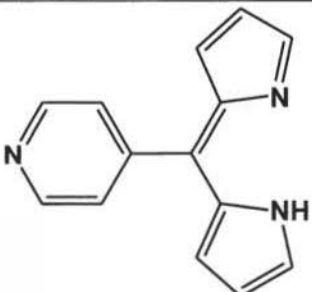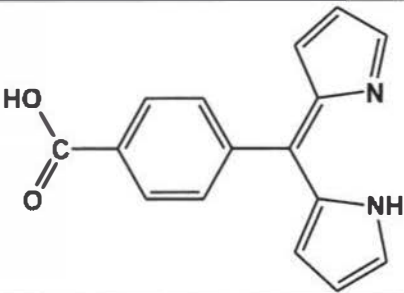
Figure I.9: Schematic representations showing interactions of metalloligands with secondary metal ions, other metalloligands, and guest; Figure from ref. 21.

Table 1.1: Examples of some ligands which can be used to synthesize metalloligands (Redrawn from reference 19).

Structure of the Ligand	Name of the Ligand
	1,3 – Bis(4-pyridyl)propane-1,3- dionato
	1,3 – Bis(3-pyridyl)propane-1,3- dionato
	3-(4-pyridyl)-2,4-pentanedionato
	3-(4-cyano)-2,4-pentanedionato
	5-(4'-pyridyl)dipyrromethene
	5-(4'-carboxyphenyl)dipyrromethene

1.3. Applications of metalloligands

One of the major challenges faced by the scientific community is to find ways to predict and, if possible, control the resultant architecture of a complex or a coordination network. Using metalloligands to construct designed materials gives several advantages over conventional method of mixing the appropriate ligand and the metal. The metalloligand approach is important to construct designed architectures, since it uses a well-defined coordination complex as the building block. Due to the precise control over the placement of appended functional groups within a metalloligand, highly ordered architectures can be obtained. A metalloligand is more rigid compared to a traditional organic ligand. Therefore, a metalloligand gives structural rigidity to the resultant network and affords firm and stable networks with permanent pores. At the same time, a metalloligand facilitates placing two or more ions in close proximity by offering binding sites to coordinate to a secondary metal ion which is advantageous especially in mimicking the active sites of various enzymes. The metalloligand approach is also very useful when designing porous materials, since it allows dual chemical functionalization of the resultant architecture by incorporating either metal or ligand based functional groups within the network.[21]

In the field of metalloligands and their use in the construction of complexes with specific functions, two strategies can be identified: the ligand centered approach and the metal centered approach.

1.3.1. The ligand-centered approach

Figure I.8 represents two metalloligands which have secondary coordination sites pointing to two different directions, therefore producing two different architectures. One could extend the structure of these metalloligands by connecting four metal ions to these secondary coordination sites. These two metalloligands generate two types of structures depending on the direction of the orientation of subsequent coordination sites, see Figure I.10.
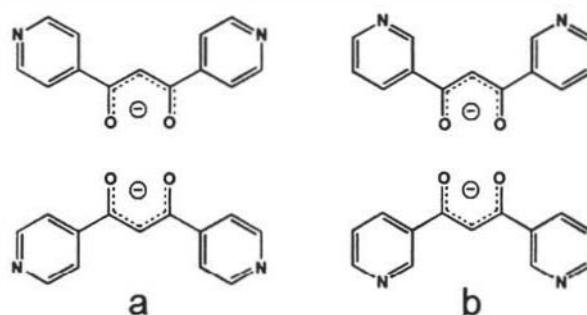
Figure I.10: a) 4-pyridyl acetylacetonate ligands; b) 3-pyridyl acetylacetonate ligands

The ligands in Figure I.10a and I.10b differ only by the position of the N atoms of the pyridine group attached to the acetonate ligand. In Figure 10a the N atom is on the 4th position of the ring while in Figure I.10b N atom is on the 3rd position of the ring. The acetyl acetonate group of these ligands acts as the primary binding site and the pyridyl rings act as the secondary binding site. Since we have two acetyl acetonate groups for each metalloligand, a four coordinate metal ions can bind with the primary binding site with the formation of a metalloligand. These and other metalloligands (for example those pictured in Figure I.11) have the N atoms oriented toward two different directions, so different structures are expected from these species.

The downfall of this ligand centered approach is that if we want to change the direction of an appended coordination site of a ligand, we have to synthesize the ligand from the beginning. Figure I.11 shows three Schiff base ligands which differ only by the position of the N atom within one pyridine ring. The coordination number of the resulting Cu complexes and the number of additional coordination sites has changed due to the change of the position of the nitrogen atom within the pyridyl ring, as pictured in Figure I.11.

Another example of metalloligands with their secondary coordination sites pointing toward different directions is shown in Figure I.12, and consist of Ru complexes of 4,4′-dicarboxy-2,2′-bipyridine and 3,3′-dicarboxy-2,2′-bipyridine. The reaction of these metalloligands with metal ions (Mg^{2+} and Sr^{2+}) produced

different architectures from each reaction, due to the difference in the direction of the coordination vector of the two carboxylate groups, see Figures 1.13 and 1.14.[22]
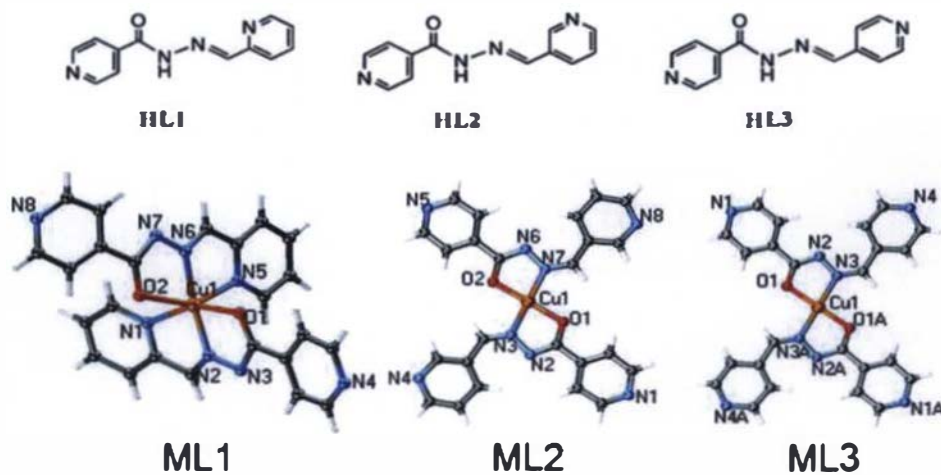
Figure I.11: Series of Isomeric Schiff Base Ligands and Copper(II) Schiff Base Metalloligands (MLs); Figure from ref. 20.
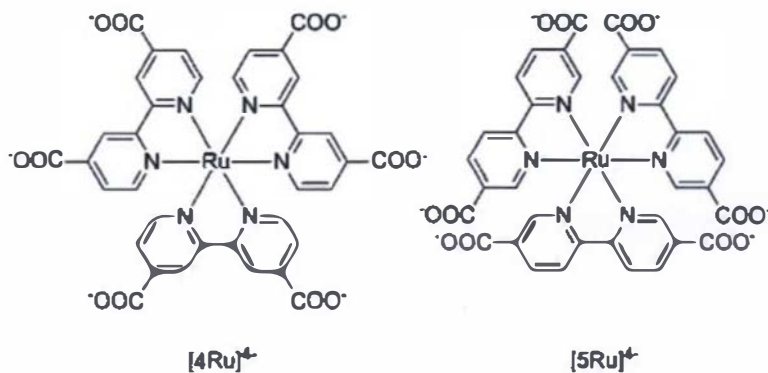
Figure I.12: Structure Representations of Isomeric Ruthenium(II) Metalloligands [4Ru] and [5Ru]; Figure from ref. 22.

13
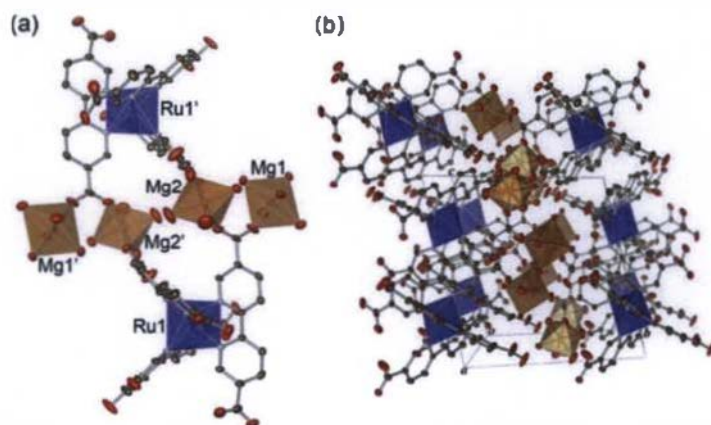
Figure I.13: a) Coordination structures of $Mg_2[5Ru] \cdot 19H_2O$ which is resulted from the reaction between Mg^{2+} and 5Ru; b) 2D layer structure of $Mg_2[5Ru] \cdot 19H_2O$ viewed along a axis. Brown, light-blue, and red ellipsoids represent C, N, and O atoms, respectively. Non-coordinated water molecules and H atoms are omitted for clarity. Figure from ref. 22.
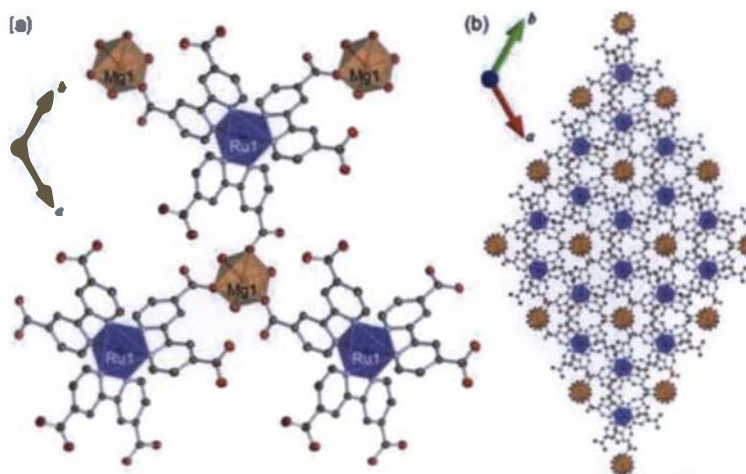
Figure I.14: a) Coordination structures of $Mg_2[4Ru] \cdot 19H_2O$ which is resulted from the reaction between Mg^{2+} and 4Ru; b) 2D layer structure of $\{[Mg(H_2O)_3][4Ru]\}$ Brown, light blue, and red ellipsoids represent C, N, and O atoms, respectively. Non-coordinated water molecules and H atoms are omitted for clarity; Figure from ref. 22.

1.3.2. Our strategy: the metal-centered approach

The metal-centered approach is illustrated in Scheme 1.2. The metal ion is surrounded by a main ligand (blue half-square in Scheme 1.2) and a labile ligand (the green half-square). One could replace this labile group by adding a suitable ditopic or tritopic ligand.

Pro-metalloligand   Metalloligand   Final complex
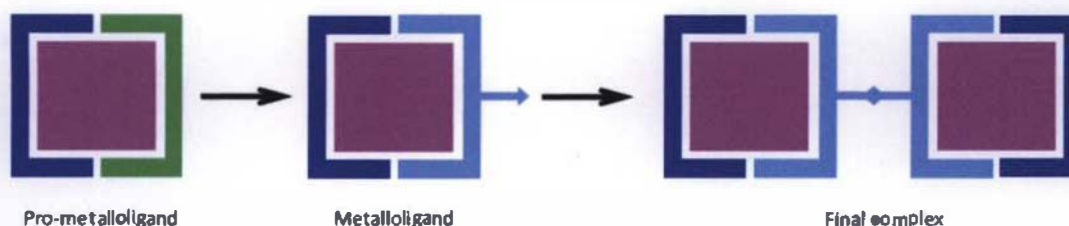
Scheme 1.2: Cartoon representation of the metalloligand synthesis used in our research.

The number of additional coordination sites available to coordinate to other metal ions would depend on the ligand which we add to replace the labile group. Therefore, we can systematically change the architecture of the extended complex by changing the second ligand, which we add to replace the labile group (see Scheme 1.2). Finally, the metalloligand can coordinate to a second metallic center, as pictured in Scheme 1.2.

To implement this approach, we followed the strategy depicted in Scheme 1.3. We have prepared a new ligand consisting of a 8-aminoquinoline core to which a bis(pyrazolyl)methane donor set was attached *via* an amide linkage. Upon deprotonation of this ligand with KOH and its subsequent reaction with a Cu(II) salt, the pro-metalloligand was obtained, consisting of a monoanionic, pentacoordinated copper(II) complex, surrounded by the four nitrogen atoms of the ligand, and a labile group filling the remaning coordination site (see the left side of Scheme 1.3). Then, several different metalloligands (see the right side of Scheme 1.3) can be prepared by replacing the labile group with various monoanionic ditopic ligands (L). Finally, the reaction of these metalloligands with other metallic salts should afford our desired dinuclear and trinuclear complexes.

15
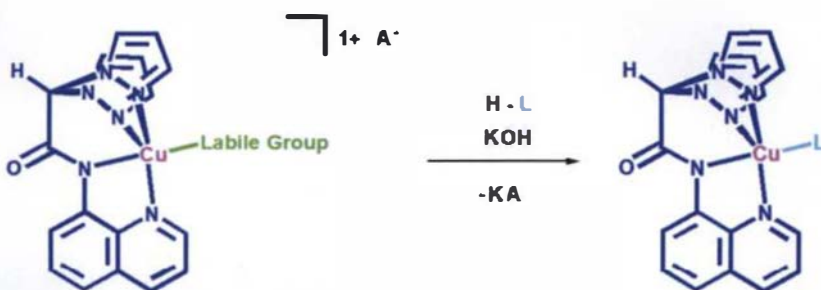
Scheme I.3: Schematic representation of our research approach for the metalloligand synthesis.

As it can be seen in Scheme I.3, we have used an amide linkage between the two coordinating sites of the ligand, and we choose this group for several reasons. We can see the amide group throughout nature, like in the primary structure of proteins. The amide group is rigid (it has a double bond), so it brings a high degree of structural predictability to the resulting metal complexes. Since amide bond is also short (there are only three bonds between the substituents of the amide group), it brings the quinoline and bis(pyrazolyl)methane groups into close proximity, so they can coordinate to the same Cu^{2+} ion easily.

References

1. https://en.wikipedia.org/wiki/Biomimetic_synthesis (accessed on 12.15.2017)

2. Marchetti, L.; Levine, M. *ACS Catal.* **2011**, *1*, 1090-1118.

3. Gavrilova, A.; Bosnich, B. *Chem. Rev.* **2004**, *104*, 349-383.

4. Schomburg, I.; Chang, A.; Placzek, S.; Sohngen, S.; Rother, M.; Lang, M.; Munaretto, C.; Ulas, S.; Stelzer, M.; Grote, A.; Scheer, M.; Schomburg, D. *Nucleic Acids Res.* **2013**, *41*, D764-D772.

5. https://www.britannica.com/science/enzyme (accessed on 11.15.2017).

6. https://en.wikipedia.org/wiki/Enzyme#cite_note-27 (accessed on 11.15.2017).

7. Karlin, K. D. *Science* **1993**, *261*, 701-708.

8. Gamez, P.; Koval, I. A.; Reedijk, J. *Dalton Trans.* **2004**, *0*, 4079-4088.

9. Solomon, E. I.; Sundaram, U. M.; Machonkin, T. E. *Chem. Rev.* **1996**, *96*, 2563-2606.

10. Kaim, W.; Rall, J. *Angew. Chem., Int. Ed.* **1996**, *35*, 43-60.

11. Guckert, J. A.; Lowery, M. D.; Solomon, E. I. *J. Am. Chem. Soc.* **1995**, *117*, 2817-2844.

12. Gastel, M. V.; Bubacco, L.; Groenen, E.J.J.; Vijgenboom, E.; Canters G.W. *FEBS Letters 474* **2000**, *2-3*, 228-232.

13. (a) Michel, H.; Behr, J.; Harrenga, A.; Kannt, A. *Annu. Rev. Biophys. Biomol. Struct.* **1998**, *27*, 329. (b) Malmstrom, B. G. *J. Biol. Inorg. Chem.* **1998**, *3*, 339. (c) Medvedev, D. M.; Daizadeh, I.; Stuchebrukhov, A. A. *J. Am. Chem. Soc.* **2000**, *122*, 228-232.

14. Lee, W.-Z.; Tolman, W. B. Inorg. Chem. **2002**, *41*, 5656-5658.

15.

https://ipfs.io/ipfs/QmXoypizjW3WknFiJnKLwHCnL72vedxjQkDDP1mXWo6uco/wiki/Nitrite_reductase.html (accessed on 11.15.2017).

16. Holland, P. L.; Tolman, W. B. *J. Am. Chem. Soc.* **1999**, *121*, 7270-7271.

17. Randall, D. W.; George, S. D.; Holland, P. L.; Hedman, B.; Hodgson, K. O.; Tolman, W.; Solomon, E. *J. Am. Chem. Soc.* **2000**, *122*, 11632-11648.

18. Tse, E. C. M.; Schilter, D.; Gray, D. L.; Rauchfuss, T. B.; Gewirth, A. A. *Inorg. Chem.* **2014**, *53*, 8505-8516.

19. https://en.wikipedia.org/wiki/Ligand (accessed on 11.15.2017).

20. Ni, W-X.; Li, M.; Zhan, S-Z.; Hou, J-Z.; Li, D. *Inorg. Chem.* **2009**, *48*, 1433-1441.

21. Kumar, G.; Gupta, R. *Chem. Soc. Rev.* **2013**, *42*, 9403-9453.

22. Kobayashi, A.; Ohba, T.; Saitoh, E.; Suzuki, Y.; Noro, S-I.; Chang, H-C.; Kato, M. *Inorg. Chem.* **2014**, *53*, 2910-2921.

II. Experimental

II.1. General Considerations

Unless otherwise noted, all operations were carried out in ambient atmosphere. Operations requiring inert (nitrogen) atmosphere were carried out using standard Schlenk techniques or using an MBraun drybox. Solvents were dried by conventional methods and distilled under a dry N_2 atmosphere immediately prior to use. NMR spectra were recorded using a 400 MHz Bruker Avance FT-NMR Spectrometer. Infrared spectroscopy was performed on a Nicolet iS10 FT-IR in a KBr matrix, and UV-Vis spectroscopic investigations were done on a Cary 100 Agilent Spectrophotometer. All other reagents used in the syntheses described below are commercially available (Sigma-Aldrich, Acros) and used without further purification.

Caution! *Although we encountered no problems during our experimental procedures, transition metal perchlorate complexes are potentially explosive and must be handled with care.*

II.2. Syntheses

The synthesis of bis(pyrazolyl)acetic acid HOOC-CH(pz)$_2$ followed the steps described in the literature.[1] 1,3-Bis(pyrazolyl)-2-butanoic acid was prepared by adapting a literature method.[2] For the sake of clarity, we describe here these steps.

II.2.1. Synthesis of HOOC-CH(pz)$_2$
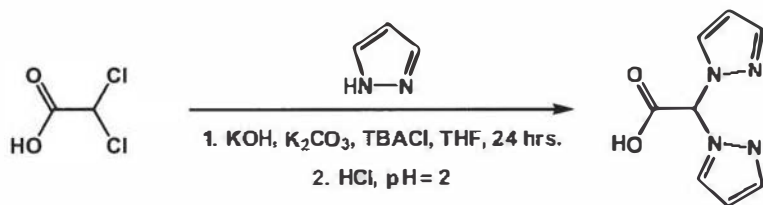
Into a three-necked, two-liter flask, equipped with an overhead mechanical stirrer and a reflux condenser, pyrazole (48.0 g, 0.705 mol), KOH (52.0 g, 0.927 mol), K$_2$CO$_3$ (125 g, 0.904 mol), benzyltriethylammonium chloride (6.0 g, 0.026 mol), and 1.3 L of THF were added. To this suspension, dichloroacetic acid (30.0 g, 0.233 mol) was carefully added, and the third neck was stoppered. The system was heated at gentle reflux with vigorous stirring overnight and then allowed to cool to room temperature.

The THF was removed *in vacuo*, and the remaining solid dried *in vacuo* overnight. One liter of water was added to give a slightly cloudy, pale yellow solution. The solution was acidified to pH 7 by careful addition of concentration HCl and then washed with diethyl ether (3 x 200 mL) to remove unreacted pyrazole. The aqueous phase was then further acidified to pH = 2. Upon brief agitation of this solution, 20.3 g of the pure desired product precipitated over approximately 30 min. and was collected by suction filtration as a white crystalline solid. The remaining aqueous filtrate was extracted with a 2.5:1 diethyl ether:THF mixture (6 x 350 mL). The combined organic extracts were dried over MgSO$_4$, and the solvent removed by rotary evaporation to yield a further 14.9 g of the crude product. Recrystallization of the crude material from a minimum amount of boiling acetone afforded a total of 30.7 g (69 %) of pure product. ^{1}H-NMR (400 MHz, Acetone-d$_6$): δ 7.99 (dd, J = 2.48 Hz, 2H, 5-pz), 7.57 (d, J = 1.48 Hz, 2H, 3-pz), 7.48 (s, 1H, -CH(pz)$_2$), 6.35 (t, J = 2.28 Hz, 2H, 4-pz).

II.2.2. Synthesis of HOOC-CH(CH$_2$-Pz)$_2$
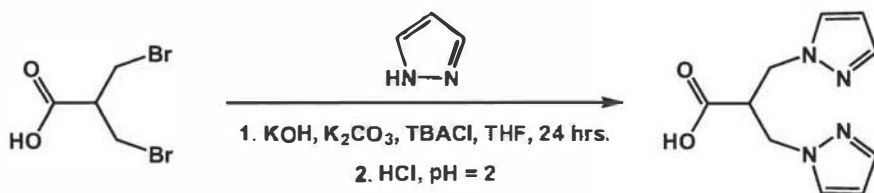
3-Bromo-2(bromomethyl)-propanoic acid (4.92 g, 20.0 mmol), pyrazole (3.41 g, 50.0 mmol), KOH (5.94 g, 90.0 mmol), K$_2$CO$_3$ (12.4 g, 90.0 mmol) and benzyltriethylammonium chloride (1.00 g) were dissolved in 100 ml of tetrahydrofuran. The reaction mixture was heated under reflux for 6 h and then the solvent was removed in vacuo. The solid residue was dissolved in 100 ml of water and the pH was adjusted to 7 with HCl. The aqueous phase was extracted with diethylether (2 x 150 ml) to remove the unreacted pyrazole. The water phase was further acidified to pH = 2. Upon brief agitation of this solution, 3.32 g of the pure desired product precipitated over approximately 30 min. and was collected by suction filtration as a white crystalline solid. Yield: 3.32 g, 75%. ^{1}H-NMR (CDCl$_3$, 400 MHz): δ 11.67 (s, 1H, -COOH), 7.67 (d, J = 2.08 Hz, 2H, 3H-*pz*), 7.47 (d, J = 1.32 Hz, 2H, 5H-*pz*), 6.24 (t, J = 2.04 Hz, 2H, 4H-*pz*), 4.43 (d, J = 1.52 Hz, CH_2), 4.42 (d, J = 1.32 Hz, 2H, CH_2), 3.62 (q, J = 6.16 Hz, 1H, CH).

II.2.3. Synthesis of HL^Q2Pz
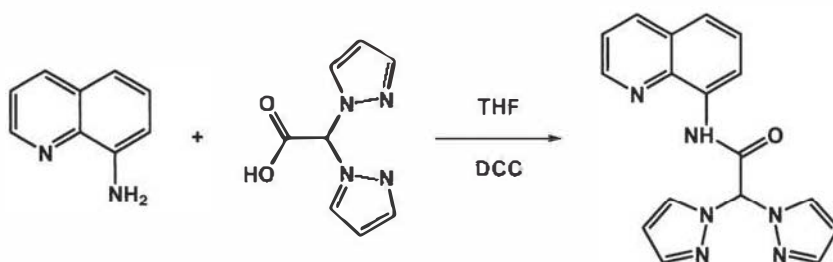
A 250 mL flask was charged with a stirring bar, 2,2'-bis(pyrazolyl)acetic acid (1.922 g, 10 mmol) and 40 mL tetrahydrofuran. To this solution, 8-aminoquinoline (1.442 g, 10 mmol) was added as a solid and kept under stirring until complete dissolution. Then, dicyclohexylcarbodiimide (DCC, 2.063 g, 10 mmol) was added as a solid. The resulting solution became cloudy and kept under stirring overnight. The formed urea was removed by filtration and volatiles removed under vacuum. The residue was taken in ethyl acetate and the organic layer was washed with brine (2 x 150 mL) and then distilled water (2 x 150 mL). The organic phase was dried over anhydrous sodium sulfate and the solvent removed under vacuum. The solid was purified by stirring the crude product in a mixture of ethyl acetate and petroleum ether (1:3 v/v) to afford the desired product as a white solid (1.97 g, 61.9 %). ^{1}H-NMR (CDCl$_3$, 400 MHz): δ 10.78 (s, br, 1H, HN-C(O)), 8.79-8.77 (m, 1H, quinoline), 8.74-8.72 (m, 1H, quinoline), 8.15-8.12 (m, 1H, quinoline), 7.86-7.85 (m, 2H, pz), 7.74-7.73 (m, 2H, pz), 7.57-7.54 (m, 2H, quinoline), 7.52-7.41 (m, 1H, quinoline), 7.28 (s, 1H, CH(pz)$_2$), 6.43-6.42 (m, 2H, pz).

II.2.4. Synthesis of [(L^•2pz)Cu(BF$_4$)]
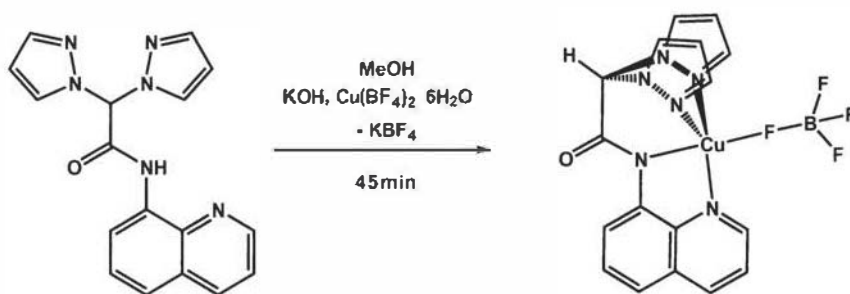
HL^Q2Pz (0.160 g, 0.5 mmol) was dissolved in MeOH (40 mL) in a 100 mL round bottom flask, equipped with a stir bar. KOH (0.850 mL, 0.51 mmol) was added and the mixture allowed to stir for 10 minutes.

20

$Cu(BF_4)_2 \cdot 6 H_2O$ (0.173 g, 0.5 mmol) was dissolved in MeOH (6 mL) and added to the flask dropwise. The solution was stirred for 45 min. The solvent was removed using rotary evaporation and the resulting powder was dried under vacuum, to afford 0.171 g (73.13 %) of the title compound as a green powder.

II.2.5. Synthesis of $[(L^Q2Pz)Cu(NCCH_3)]ClO_4$
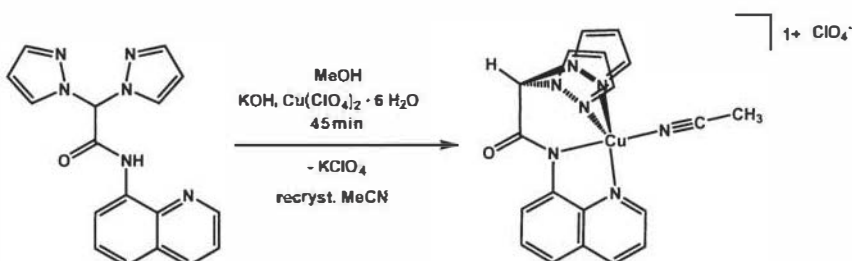
HL^Q2Pz (0.318 g, 1.0 mmol) was dissolved in MeOH (30 mL) in a 100 mL flask equipped with a stir bar. KOH (1.664 mL, 1.0 mmol) was added and the mixture was stirred for 10 minutes. $Cu(ClO_4)_2 \cdot 6 H_2O$ (0.371 g, 1.0 mmol) was dissolved in MeOH (20 mL) and then added to the flask. The solution turned from light yellow to green. The solution was stirred for 45 min. The methanol was removed using rotary evaporation and the resulting powder was dried under vacuum for one hour. The resulting solid was redissolved in dry acetonitrile. The undissolved $KClO_4$ was removed by filtration, and the title compound was obtained as a green powder after removing the solvent in 93.6 % yield (0.488 g).

II.2.6. Synthesis of $[(L^Q2pz)Cu(O_2C-CH_3]$
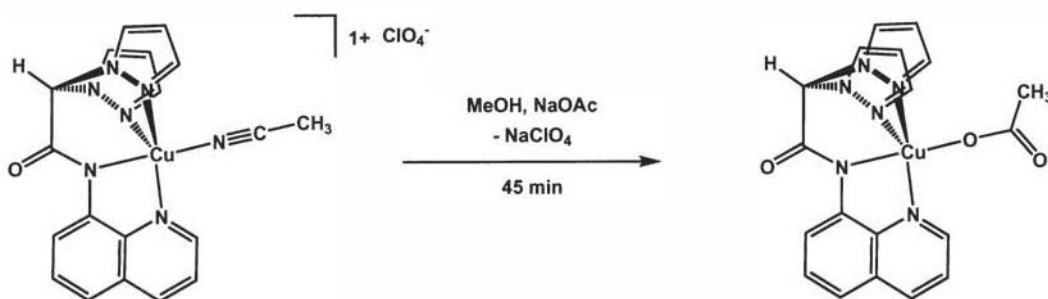
$[(L^Q2Pz)Cu(NCCH_3)]ClO_4$ (0.130 g, 0.25 mmol) and CH_3COONa (0.021 g, 0.25 mmol) was dissolved in MeOH (20 mL) in 100 mL round bottom flask equipped with a stir bar. The solution was stirred for 45 minutes. The solvent was evaporated using rotary evaporation and the resulting powder was kept under

vacuum for one hour. The solid was taken in dichloromethane and filtered (to remove the formed NaClO₄) into a clean 100 mL flask. Removal of the solvent afforded the title compound (0.082 g, 75.2 %) as a green powder.

II.2.7. Synthesis of [(L^Q2Pz)Cu(O₂C-CH₂-Py)]
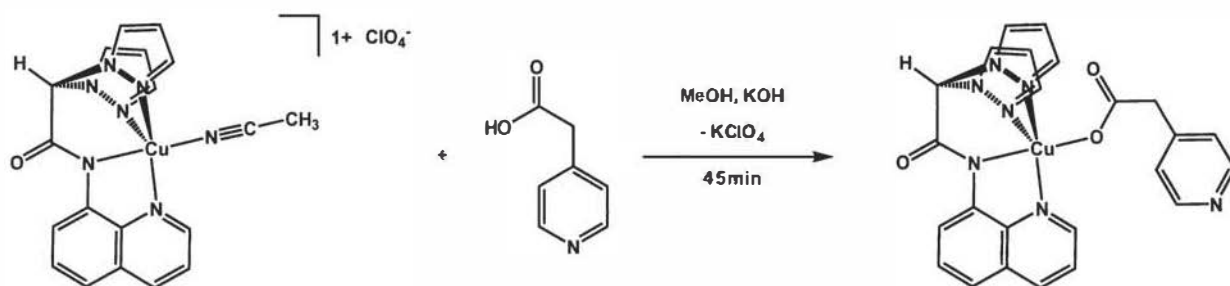
[(L^Q2Pz)Cu(NCCH₃)]ClO₄ (0.198 g, 0.38 mmol) was dissolved in MeOH (30 mL) in a 100 mL flask equipped with a stir bar. 4-Pyridyl acetic acid (0.052g, 0.38 mmol) was added into the flask while stirring. KOH (0.632 mL, 0.38 mmol) was added to the flask and the mixture was stirred for 45 minutes. The solvent was removed using rotary evaporation and the solids were kept under vacuum for one hour. The product was dissolved in dichloromethane, and the mixture was filtered to remove the formed KClO₄. Removal of the solvent afforded 0.121 g (61.59 %) of the title compound as a green powder.

II.2.8. Synthesis of [(L^Q2pz)Cu(O₂C-CH-pz₂)]
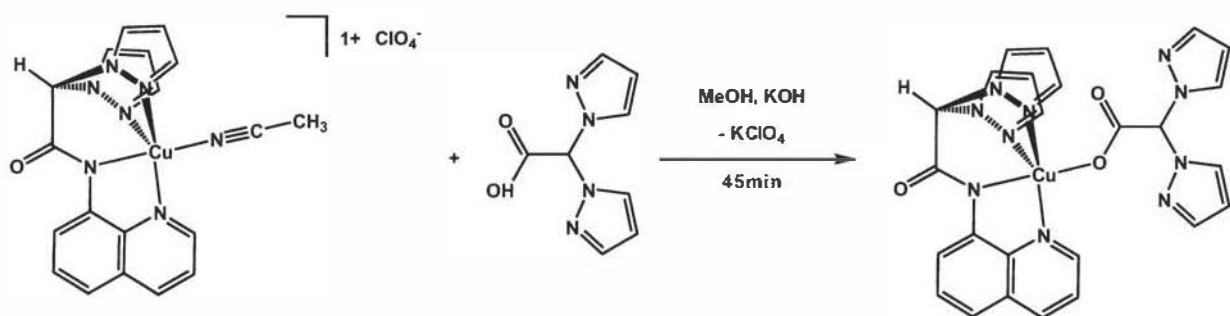
[(L^Q2Pz)Cu(NCCH₃)]ClO₄ (0.130 g, 0.25 mmol) and 2,2'-bis(pyrazolyl)acetic acid (0.048 g, 0.25 mmol) were dissolved in MeOH (20 mL) in a 100 mL round bottom flask equipped with a stir bar. KOH (0.416 mL of a 0.6 M solution, 0.25 mmol) was added to a round bottom flask while stirring. The solution

was stirred for 45 minutes. The solvent was removed under vacuum. The product was dissolved in dichloromethane, and the mixture was filtered to remove the formed KClO₄. Removal of the solvent afforded 0.087 g (60.83 %) of the title compound as a green powder.

II.2.8. Synthesis of [(L^{Q}2pz)Cu(O₂C-CH(CH₂pz)₂)]
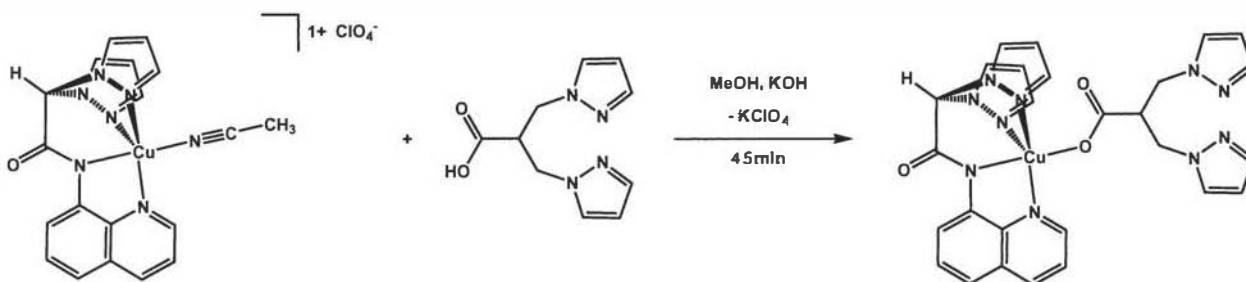
[(L^{Q}2Pz)Cu(NCCH₃)]ClO₄ (0.130 g, 0.25 mmol) and 2-methylpyrazolyl-3-pyrazolyl propanoic acid (0.055 g, 0.25 mmol) was dissolved in MeOH (20 mL) in 100 mL RBF equipped with a stir bar. KOH (0.416 mL of a 0.6 M solution, 0.25 mmol) was added to a round bottom flask while stirring. The solution was stirred for 45 minutes. The solvent was removed under vacuum. The product was dissolved in dichloromethane, and the mixture was filtered to remove the formed KClO₄. Removal of the solvent afforded 0.098 g (65.32 %) of the title compound as a green powder.

II.2.9. Synthesis of [(L^{Q}2pz)Cu(O₂C-CH(CH₂-pz)₂)]₂Cu(PF₆)
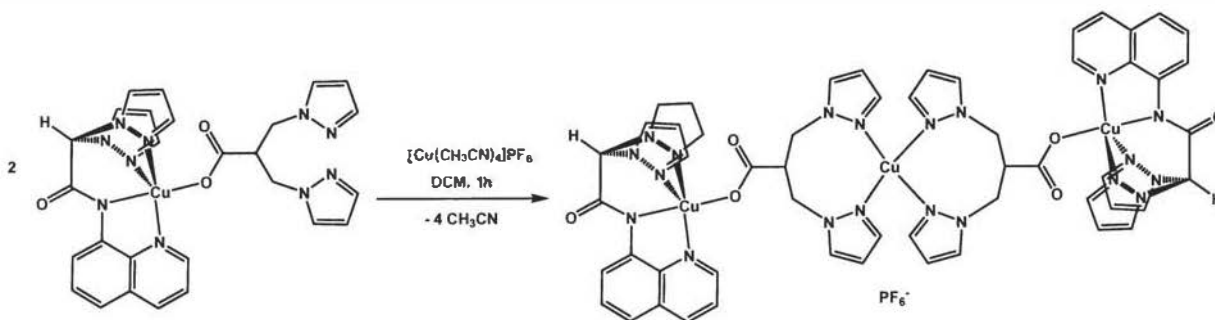
In a drybox, [(L^{Q}2pz)Cu(O₂C-CH(CH₂pz)₂)] (0.050 g, 0.08 mmol) and Cu(CH₃CN)₄PF₆ (0.016 g, 0.04 mmol) were dissolved in dichloromethane (20 mL) and added to a 100 mL RBF equipped with a stir bar.

The solution was stirred for 1 hr. Removal of the solvent afforded 0.047 g (83.9 %) of the title compound as a green powder.

II.2.10. Synthesis of [(L^{Q}2pz)Cu(O$_2$C-CH(CH$_2$-pz)$_2$Cu(PPh$_3$)$_2$]NO$_3$
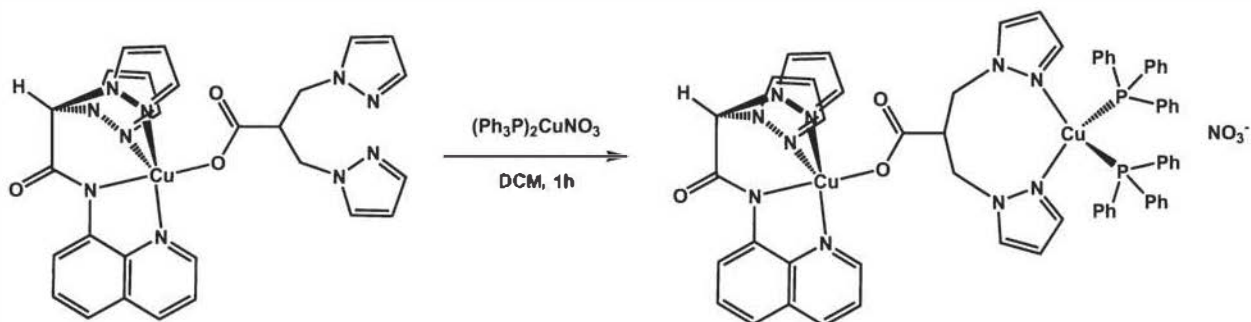
[(L^{Q}2pz)Cu(O$_2$C-CH(CH$_2$pz)$_2$)] (0.060 g, 0.1 mmol), (Ph$_3$P)$_2$CuNO$_3$ (0.065 g, 0.1 mmol) were dissolved in dichloromethane (50 mL) and added to a 100 mL RBF equipped with a stir bar. The solution was stirred for 1 hr. Removal of the solvent afforded 0.102 g (81.6 %) of the title compound as a green powder.

II.3. X-ray Crystallography

The X-ray data were collected at 100 K on a Bruker SMART APEXII CCD diffractomer equipped with Cu-Kα radiation. Intensities were collected using phi and omega scans and were corrected for Lorentz polarizatrion and absorption effects. The *X-SEED* software platform[3] equipped with *SHELXS* and *SHELXL* modules on a PC computer,[4] was used for all structure solution and refinement calculations and molecular graphics. The structure was solved by direct methods, and refined by anisotropic full-matrix least-squares for all non-hydrogen atoms. All hydrogen atoms were placed in calculated positions and refined using a riding model with fixed thermal parameters.

References

1. Reger, D. L.; Foley, E. A.; Semeniuc, R. F.; Smith, M. D. *Inorg. Chem.* **2007**, *46*, 11345.

2. Kozlevcar, B.; Golobic, A.; Gamez, P.; Koval, I. A.; Driessen, W. L.; Reedijk, J. *Inorg. Chim. Acta.* **2005**, *358*, 1135.

3. Barbour, L. J. *Supramol. Chem.* **2001**, *1*, 189.

4. Sheldrick, G. M. *Acta Crystallogr.* **2008**, *A64*, 112.

III. Results and Discussion

III.1. Ligand Design, Synthesis, and Characterization

In the design of our new ligand, we chose the quinoline to be the main "body" of the ligand, since this group is known to coordinate to the metallic center.[1] We used the bis(pyrazolyl)methane group as the donor set (-C(pz)$_2$, pz = pyrazolyl ring), since this group is known for its coordination abilities,[2,3] and an amide moiety as a linker between the -C(pz)$_2$ region and the body of the ligand. Our choice for the amide group stems from several reasons. First, the -NHC(O)- linkage is rigid and robust, as demonstrated by the protein architectures capable of performing complex tasks in biological systems.[4] Second, the amide group can bind to metallic centers *via* the oxygen atom in the case of neutral amides, or *via* the nitrogen atom in the case of deprotonated amides.[5,6] The synthesis of the ligands is described in Scheme III.1. and we will refer to it as **L^{Q}2Pz**. The L^{Q}2Pz ligand was prepared by the dicyclohexylcarbodiimide (DCC) assisted reaction between the bis(pyrazolyl)methane acetic acid and 8-aminoquinoline. The ligand was isolated as a white powder in good to very good yields.
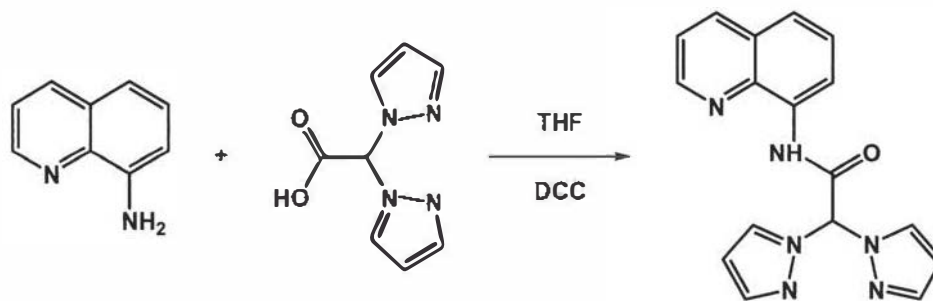
Scheme III.1. The synthetic pathway toward the HL^{Q}2Pz ligand.

The ^{1}H-NMR spectrum of the HL^{Q}2Pz ligand is presented in Figure III.1., and it shows the expected proton resonances for the structure of the ligand. The IR spectrum of the ligand is also in agreement with

26

the structure of the ligand. In this work, two stretching vibrations of the ligand are of interest: the v_{NH} and v_{CO} stretching vibrations, which appear at 3298.68 cm^{-1} and 1715.28 cm^{-1}, respectively, see Figure III.2.
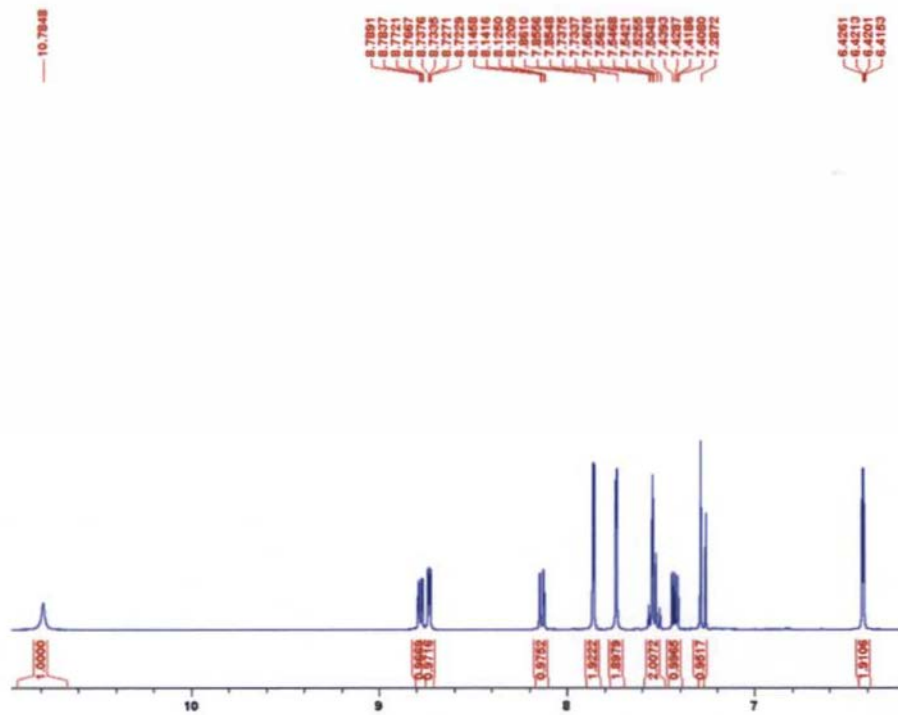
Figure III.1. The ^{1}H-NMR spectrum of the HL^{Q}2Pz ligand.
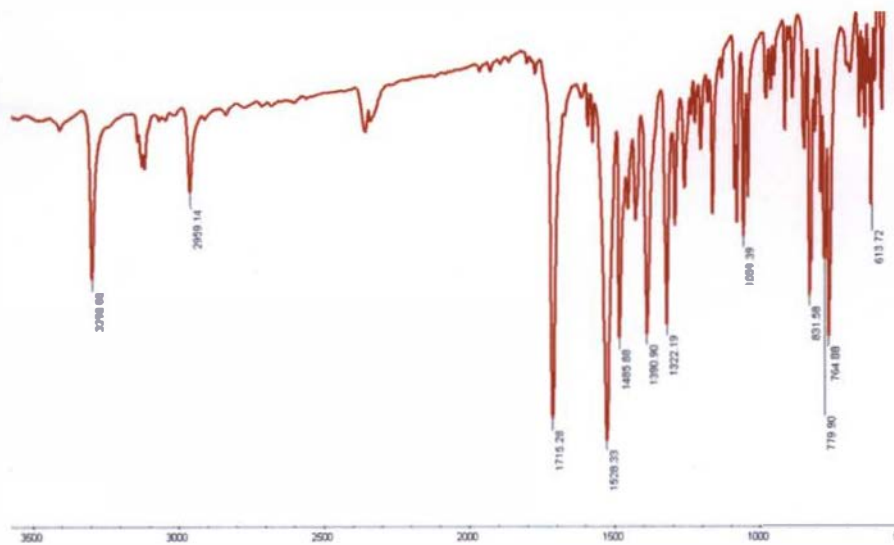
Figure III.2. The IR spectrum of the HL^{Q}2Pz ligand.

III.2. Pro-metalloligands: Design, Syntheses, and Characterization

In order to prepare a pro-metalloligand, we needed a copper(II) starting material with a non-coordinating anion. The concept is depicted in Scheme III.2.: upon the deprotonation of the amide region of the ligand, the copper(II) center would be coordinated by the quinoline N atom, the amide N atom, and the bis(pyrazolyl)methane donor set of the ligand. The remaining coordination site of the Cu^{2+} ion would be occupied by a labile group (e.g. a solvent molecule with coordinating properties like acetonitrile), which can be easily replaced by a secondary di- or tritopic ligand, as pictured on the right side of Scheme III.2.
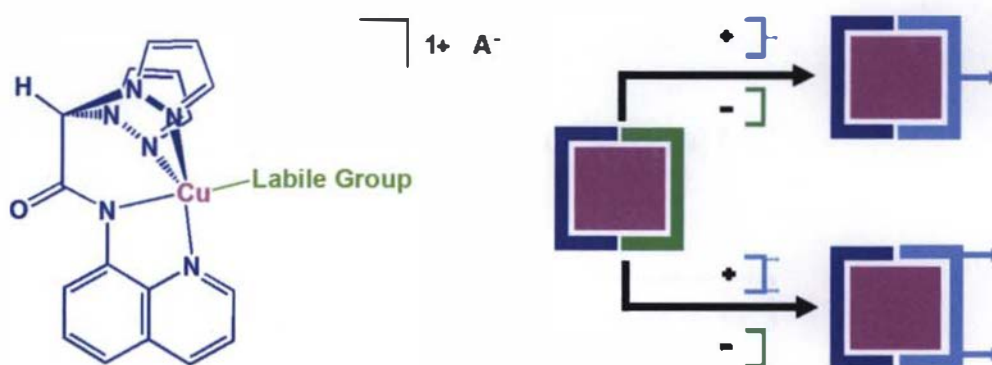
Scheme III.2. The concept of a pro-metalloligand and the resulting metalloligands.

III.2.1. (L^{Q}2Pz)CuBF$_4$

Our first attempt to synthesize a pro-metalloligand involved the reaction between our quinoline ligand and copper(II) tetrafluoroborate, $Cu(BF_4)_2 \cdot 6\ H_2O$. Usually, the BF_4^- anion has weak donor capabilities, and is rarely coordinated to the metal center. To prepare the copper complex, the following strategy was applied: the ligand was dissolved in methanol and deprotonated by the addition of one equivalent of base, followed by the addition of one equivalent of $Cu(BF_4)_2 \cdot 6\ H_2O$. The IR spectrum of the product (see Figure III.3.) showed that indeed the deprotonation of the ligand was successful (the peak at 3298 cm^{-1} disappeared) and the coordination of the amide group to the copper center took place (the $v_{C=O}$ stretching vibration shifted from 1715 cm^{-1} to 1607 cm^{-1})
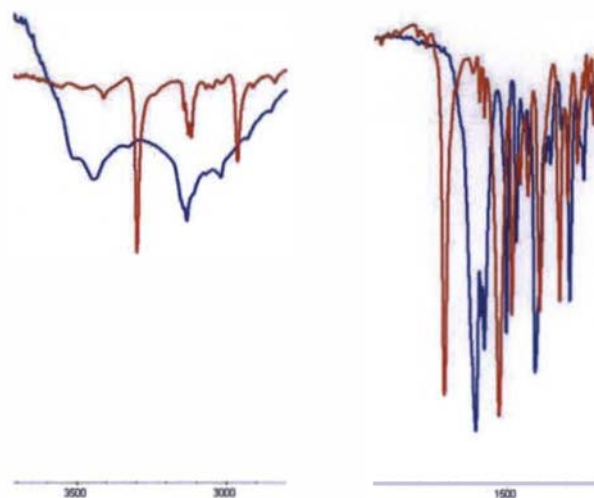
Figure III.3. IR spectrum of HL^Q2Pz (red) and $(L^Q2Pz)Cu(BF_4)$ (blue) highlighting the differences between the free ligand and its copper complex.

The UV-Vis spectrum of the complex (Figure III.4.) also indicated the formation of the desired complex: the d-d transition, observed at 670 nm, suggests the formation of a pentacoordinated copper(II) center in a square pyramidal geometry.
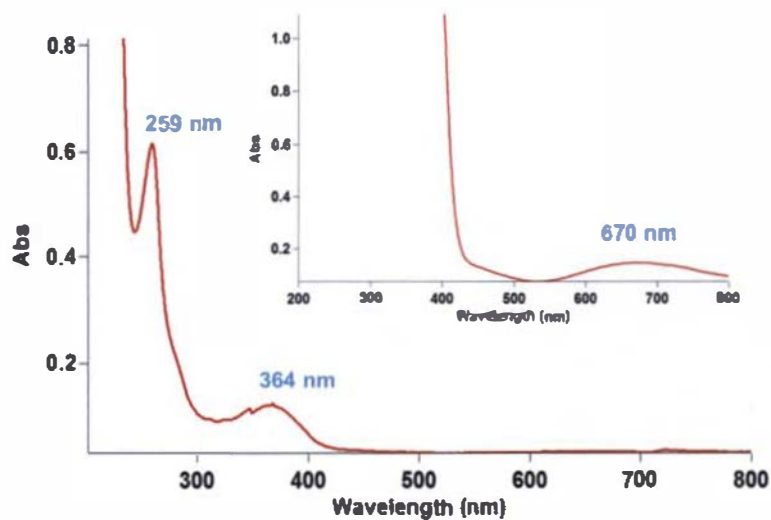
Figure III.4. UV-Vis spectrum of $(L^Q2Pz)Cu(BF_4)$.

To confirm the structure of the complex, single crystals were grown and subjected to X-ray diffraction experiments. The structure of the complex is depicted in Figure III.5. While the structural characterization confirmed the pentacoordination of the copper center, unfortunately the BF_4^- anion was found to be coordinated to the copper ion. Selected bond lengths and angles are given in Table III.1. The crystal structure reveals that there is one independent molecule per asymmetric unit. In this complex, each copper ion is five coordinated, and bound to one deprotonated nitrogen atom from the amide group, one fluorine atom from the tetrafluoroborate anion, two nitrogen atoms from the two pyrazolyl rings and one nitrogen atom from the quinoline.
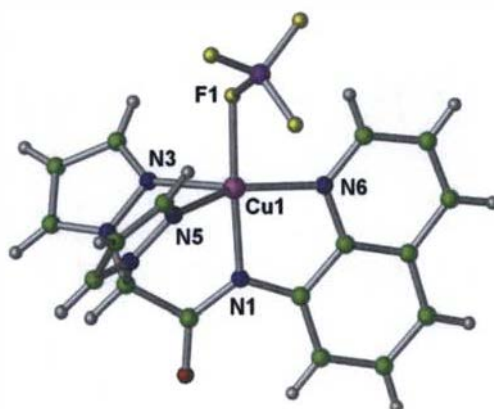
Figure III.5. Molecular structure of $(L^Q2Pz)Cu(BF_4)$.

Table III.1. Selected bond lengths (Å) and angles (°) for $(L^Q2Pz)Cu(BF_4)$.

Atoms	Bond lengths	Atoms	Bond Angles
Cu1-F1	1.975	F1-Cu1-N1	176.93
Cu1-N1	1.986	F1-Cu1-N3	94.40
Cu1-N3	2.194	F1-Cu1-N5	93.16
Cu1-N5	2.070	F1-Cu1-N6	94.71
Cu1-N6	2.003	N1-Cu1-N3	86.67
		N1-Cu1-N5	89.76
		N1-Cu1-N6	82.33
		N5-Cu1-N3	86.81
		N6-Cu1-N3	125.10
		N6-Cu1-N5	146.25

The geometry around copper is in between trigonal bipyramidal and square pyramidal, as it can be seen in Figure III.6. In the case of five-coordinated complexes, which can have either a trigonal bipyramidal or a square pyramidal geometry, the degree of distortion from the ideal geometry is described by the angular parameter τ_5.[7] This parameter is calculated by dividing the difference between the two largest angles by 60; a trigonal bipyramidal structure would produce a value of 1, while a square pyramidal structure would produce a value of 0. For this complex, the τ_5 value is 0.51, clearly indicating a distortion from the ideal geometries. All of complexes described here have similar environments (*vide infra*), between a trigonal bipyramid (TBP) and square pyramid (SP); however, in order to simplify the discussion, we will treat all complexes as having a trigonal bipyramidal geometry. In the case of $L^Q2PzCu(BF_4)$, the equatorial coordination sites are occupied by N3, N5 and N6 atoms, while the axial coordination sites are occupied by N1 and F1. The distances between Cu1-N1, Cu1-F1 are 1.986 Å and 1.975 Å. The corresponding N1-Cu1-F1 bond angle is 176.93°. The distances between Cu1-N3, Cu1-N5 and Cu1-N6 are 2.194 Å, 2.070 Å and 2.003 Å, respectively. The bond angles of N3-Cu1-N6 and N5-Cu1-N6 are 125.1° and 146.25° respectively. The small bite angle (86.81° for N3-Cu1-N5) of the chelating bis(pyrazolyl)methane group is the main factor accounting for this distortion from ideal trigonal bipyramidal geometry.
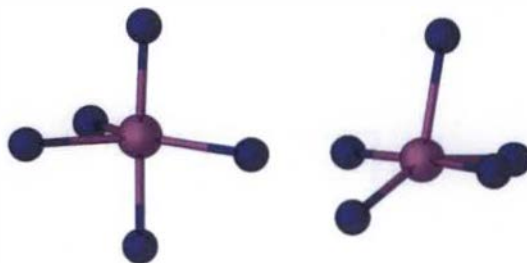
Figure III.6. Two views of the environment around Cu(II) centers in $(L^Q2pz)Cu(BF_4)$, emphasizing the TBP (left) and SP (right) geometries.

Figure III.7. depicts the intermolecular π-π stacking interactions in a dimer of $[(L^Q2pz)Cu(BF_4)]_2$, and shows three such dimers built by relatively strong π-π stacking interactions (the quinoline centroid-centroid

distance is 3.694 Å, while the perpendicular inter-plane separation is 3.455 Å) and held together by slightly weaker interactions (the corresponding centroid-centroid distance is 3.842 Å, and the perpendicular inter-plane separation is 3.690 Å) between two dimers. The quinoline rings of both molecules of the dimer act as hydrogen donors in C-H⋯π interactions between the quinoline rings and the pyrazolyl rings (C-H⋯centroid angle of 137.92^0 and a H-centroid distance of 2.998 Å). The overall crystal structure of the complex is depicted in Figure III.8.
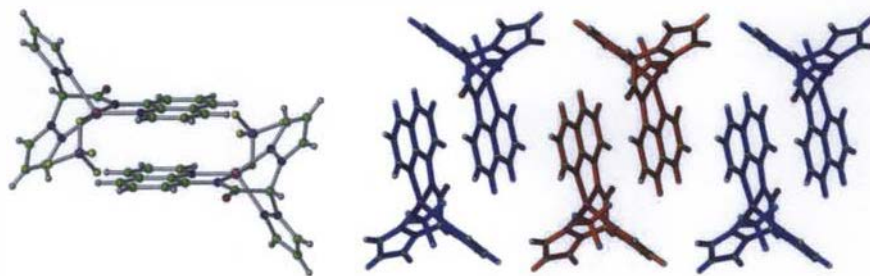
Figure III.7. a) Intermolecular π-π stacking interactions in (L^{Q}2pz)Cu(BF$_4$)] forming [L^{Q}2PzCu(BF$_4$)]$_2$ dimers; b) chain formation via successive π-π stacking / C-H⋯π interactions between [L^{Q}2PzCu(BF$_4$)]$_2$ dimers.
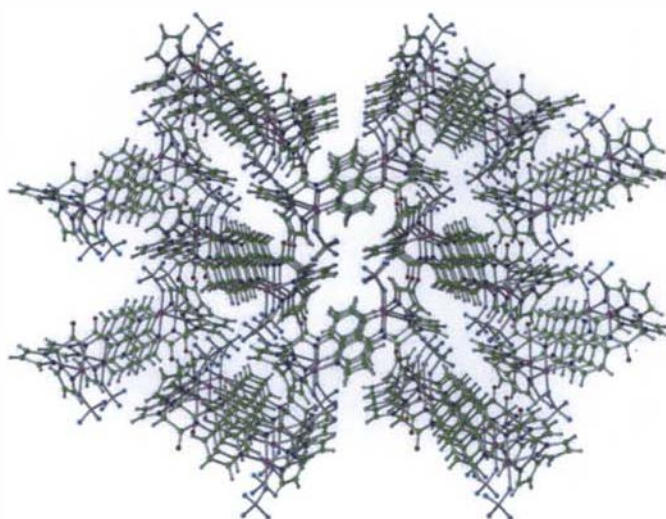
Figure III.8. View of the crystal packing of (L^{Q}2pz)Cu(BF$_4$) along a axis.

III.2.2. (L^{Q}2Pz)Cu(NCCH$_3$)]ClO$_4$

Since we have found the tetrafluoroborate anion coordinated to the Cu(II) center, we turned our attention to another non-coordinating species, the perchlorate anion. The reaction between the ligand and Cu(ClO$_4$)$_2$ · 6 H$_2$O in the same conditions and above, yielded a green compound having similar IR and UV-Vis spectra (see Figures III.9. and III.10, respectively). As before, the IR spectrum clearly suggests the coordination of the amide group to the copper center, while the UV-Vis spectrum indicates the formation of a square pyramidal geometry around the copper(II) ion.

Figure III.9. IR spectrum of HL^{Q}2Pz (red) and [(L^{Q}2Pz)Cu(NCCH$_3$)]ClO$_4$ (blue) highlighting the differences between the free ligand and its copper complex.

Figure III.10. UV-Vis spectrum of [(L^{Q}2Pz)Cu(NCCH$_3$)]ClO$_4$.

33

X-Ray diffraction experiments revealed that indeed the perchlorate anion is not coordinated to the copper(II) ion. The structure of $[(L^Q2Pz)Cu(NCCH_3)]ClO_4$ is shown in Figure III.11 and selected bond lengths and angles given in Table III.2. The crystallographic analysis revealed that there is one independent complex per asymmetric unit. The ClO_4^- ion acts as a counter-ion and resides close to the ligating acetonitrile and above one of the pyrazolyl rings. In this complex, the copper(II) ion is five coordinated and bound to one deprotonated nitrogen atom from the amide group, one nitrogen atom from the acetonitrile, two nitrogen atoms from two pyrazolyl rings and one nitrogen atom from the quinoline moiety.

The geometry around copper is again between trigonal bipyramidal and square planar, with the τ_5 parameter having the value of 0.46. Considering the trigonal bipyramidal geometry, the equatorial sites of Cu1 are occupied by the N1 atom from the quinoline group and the N4 and N6 atoms from pyrazolyl rings, while axial sites are occupied by N2 atom from the amide and the N7 atom from the acetonitrile molecule. The distances between Cu1-N1, Cu1-N4 and Cu1-N6 are 2.0033 Å, 2.1963 Å and 2.0880 Å, respectively. The distances between Cu1-N2 and Cu1-N7 are similar, around 1.96 Å. The equatorial bond angles N1-Cu1-N4, N4-Cu1-N6, and N1-Cu1-N6 are 123.77°, 85.11° and 149.30°, respectively, while the axial bond angle N2-Cu1-N7 is 177.18°.

Table III.2. Selected bond lengths (Å) and angles (°) for $[(L^Q2Pz)Cu(NCCH_3)]ClO_4$.

Atoms	Bond lengths	Atoms	Bond Angles
Cu1-N1	2.0033	N1-Cu1-N4	123.77
Cu1-N2	1.9607	N1-Cu1-N6	149.30
Cu1-N4	2.1963	N2-Cu1-N1	82.40
Cu1-N6	2.0880	N2-Cu1-N4	87.15
Cu1-N7	1.9613	N2-Cu1-N6	89.66
		N2-Cu1-N7	177.18
		N6-Cu1-N4	85.11
		N7-Cu1-N1	95.01
		N7-Cu1-N4	95.23
		N7-Cu1-N6	92.04
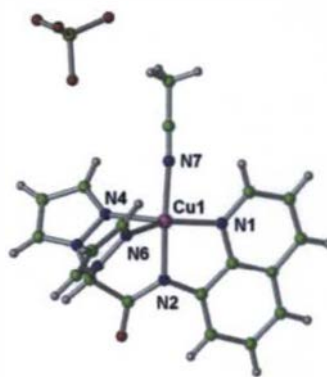
Figure III.11. Structural details of [(L^Q2Pz)Cu(NCCH₃)]ClO₄.

Figure III.12 shows three dimers with relatively strong π-π stacking interactions (centroid···centroid distance is 3.460 Å, and the perpendicular inter-plane separation is 3.353 Å) between the quinoline rings of the dimer. In the same time, the quinoline rings act as a hydrogen donor to one of the pyrazolyl rings of the other molecule of the dimer, forming C-H···π interactions (the C-H···centroid angle is 147.02° and the H-centroid distance is 3.203 Å) between the two molecules of the dimer. Another interaction involves the bis(pyrazolyl)methane groups, also involved in similar π-π and C-H···π interactions, as described above and pictured at the right of Figure III.12. Two pyrazolyl rings are involved in π-π stacking interactions, and also act as hydrogen donors in a C-H···π interactions (with a C-H···centroid angle of 104.10° and a H···centroid distance of 3.387 Å).
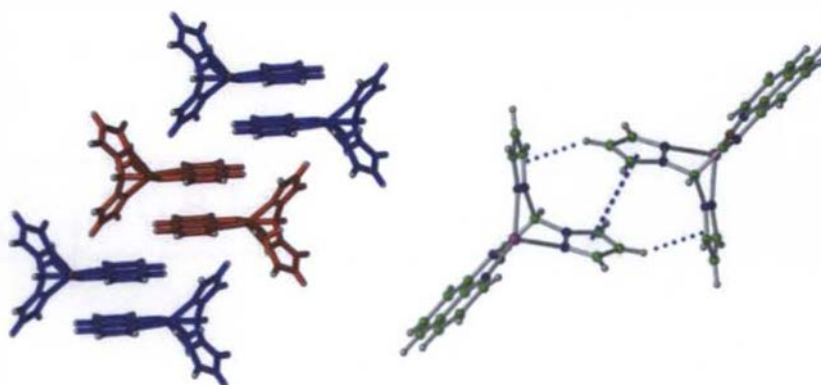
Figure III.12. Non-covalent forces in [(L^Q2Pz)Cu(NCCH₃)]ClO₄: a) π-π stacking interactions between two {[(L^Q2Pz)Cu(NCCH₃)]⁺}₂ dimers and b) the pyrazolyl embrace between two [(L^Q2Pz)Cu(NCCH₃)]⁺ moieties (acetonitrile molecules were removed for clarity purposes).

These interactions build up the extended structure of $[L^Q2PzCu(NCCH_3)](ClO_4]$, consisting of polymeric chains which propagate along the b axis (see the top of Figure III.13.). The perchlorate counter-ions reside between these chains, but for clarity purposes are not shown in the Figure. The bottom part of Figure III.13. shows the crystal packing of four such chains, building up the crystal packing of $[L^Q2PzCu(NCCH_3)](ClO_4]$.
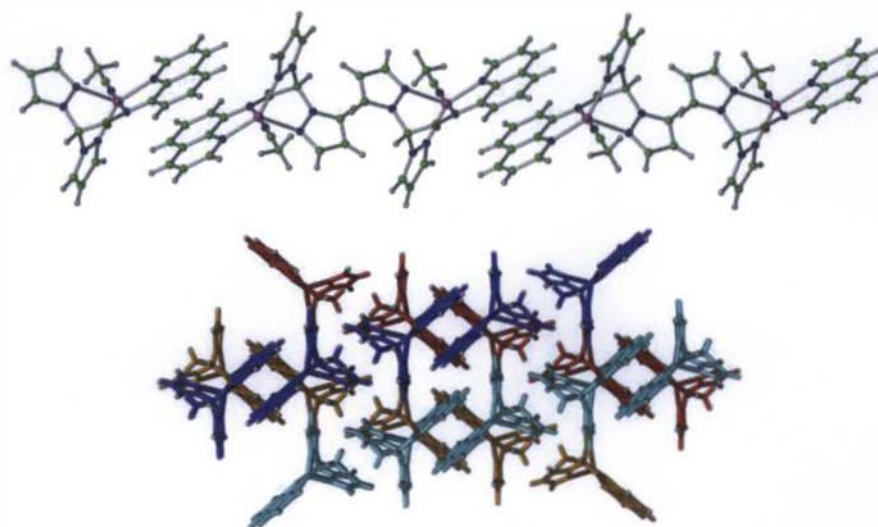
Figure III.13. Crystal packing of $[(L^Q2Pz)Cu(NCCH_3)]ClO_4$: a) view of the supramolecular polymeric chain of $[(L^Q2Pz)Cu(NCCH_3)]^+$ cations which propagate along b axis; b) four such chains, building up the crystal packing of $[(L^Q2Pz)Cu(NCCH_3)]ClO_4$; ($ClO_4^-$ ions were removed for clarity purposes).

III.2.3. $(L^Q2Pz)Cu(OAc)$

Once the pro-metalloligand was successfully prepared, we tested its behavior to act as a starting material in the synthesis of various metalloligands, without using expensive starting materials. Therefore, we have studied the reaction between $[(L^Q2Pz)Cu(NCCH_3)]ClO_4$ and sodium acetate, to form the model complex $(L^Q2Pz)Cu(OAc)$. After removal of the formed sodium perchlorate, a green compound was isolated. The IR spectrum of the complex (Figure III.14.) clearly proves that amide group is still coordinated to the copper center, while the UV-Vis spectrum (Figure III.15.) indicates that the square pyramidal geometry around the copper(II) ion is maintained in this complex.
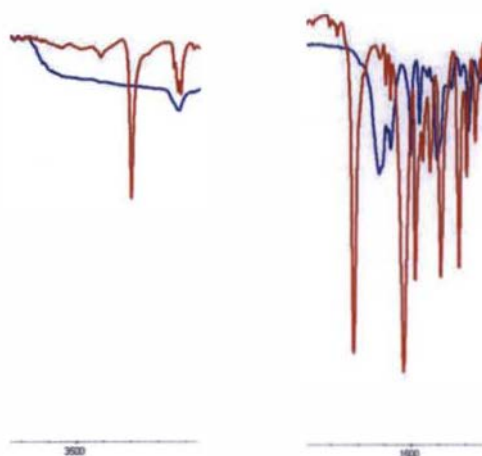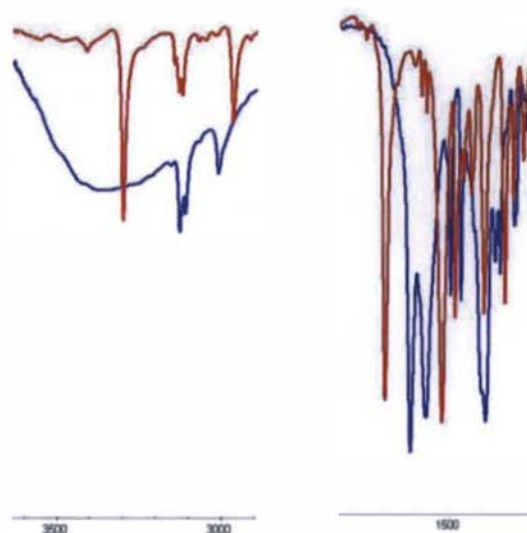
Figure III.14. IR spectrum of HL^{Q}2Pz (red) and (L^{Q}2Pz)Cu(OAc) (blue) highlighting the differences between the free ligand and its copper complex.

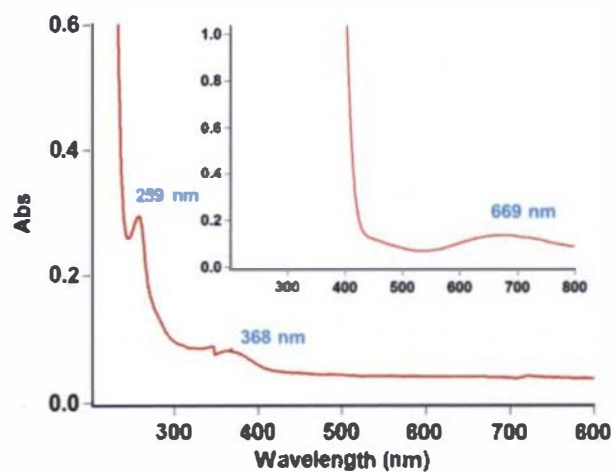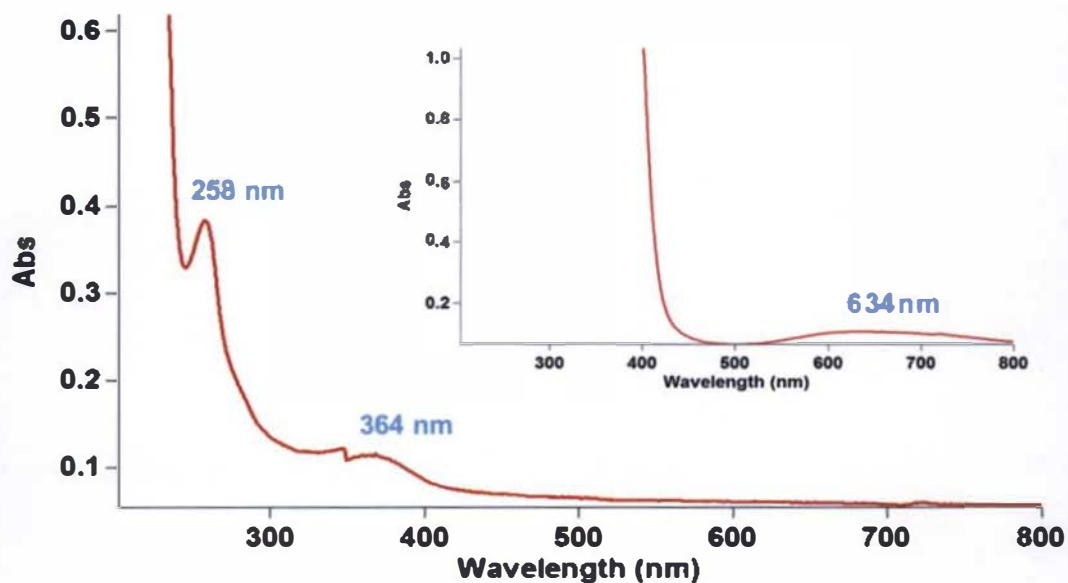**Figure III.15.** UV-Vis spectrum of (L^{Q}2Pz)Cu(OAc).

X-Ray diffraction experiments revealed that there are two independent molecules per asymmetric unit. The molecular structure of one (L^{Q}2pz)Cu(OAc) molecule is shown in Figure III.16. and selected bond lengths and angles are given in Table III.3. Each copper ion is five-coordinated and bound by one

deprotonated nitrogen atom from the amide group, one oxygen atom from the acetate ligand, two nitrogen atoms from the two pyrazolyl rings and one nitrogen atom from the quinoline moiety. The bond distances and angles of the two independent molecules (A and B) show no significant differences between the two species.

The geometry around the copper ion in complex A and B is in between trigonal bipyramidal and square planar, with the τ_5 parameters having the values of 0.36 and 0.49. Considering the trigonal bipyramidal geometry, in complex A the equatorial sites of Cu1A are occupied by the N1A atom from the quinoline moiety and the N3A and N5A atoms from the pyrazolyl rings, while the axial sites are occupied by N2A atom from the amide group and the O2A atom from the acetate ligand. The distance between Cu1A-N1A, Cu1A-N3A and Cu1A-N5A are 1.999 Å, 2.032 Å and 2.329 Å, respectively. The distance between Cu1A-N2A and Cu1A-O2A are 1.968 Å and 1.942 Å, respectively. The equatorial bond angles between N1A-Cu1A-N3A, N3A-Cu1A-N5A, N1A-Cu1A-N5A are 155.30°, 84.95° and 117.22°, respectively, while the axial bond angle of N2A-Cu1A-O2A is 177.07°.

The equatorial sites of Cu1B in complex B are occupied by the N3B and N5B atoms from the pyrazolyl rings and the N1A atom from the quinoline moiety, while axial sites are occupied by the N2B and O2B atoms. The distance between Cu1B-N1B, Cu1B-N3B and Cu1B-N5B are 2.006 Å, 2.089 Å, and 2.236 Å, respectively. The distance between Cu1B-N2B and Cu1B-O2B are 1.974 Å and 1.928 Å. The equatorial bond angles of N1B-Cu1B-N3B, N3B-Cu1B-N5B, N1B-Cu1B-N5B are 144.92°, 84.81° and 127.71°, respectively, while the axial bond angle of N2A-Cu1A-O2A is 174.10°.

Figure III.16. also depicts the intermolecular H-bonding interactions between four molecules of $(L^Q2pz)Cu(OAc)$ forming a tetramer. There are six H-bonding interactions per each tetramer. Two water molecules participate in four of H-bonding interactions. The distances between H-bonding interactions of O3A···H2, O2B···H1, O3B···H11A are 2.202 Å, 1.838 Å, and 2.184 Å, respectively. The angles between O1-H1-O2B, C11A-H11A-O3B, and O1-H2-O3A are 155.49°, 156.95° and 170.27°, respectively.

Table III.3. Selected bond lengths (Å) and angles (°) for (L^{Q}2pz)Cu(OAc).

Atoms	Bond lengths	Atoms	Bond Angles
CulA-NIA	1.999	N1A-CulA-N3A	155.30
Cul A-N2A	1.968	N1A-Cul A-N5A	117.22
Cul A-N3A	2.032	N2A-CulA-N1A	82.22
Cul A-N5A	2.329	N2A-CulA-N3A	89.52
Cul A-O2A	1.942	N2A-Cul A-N5A	85.05
		N3A-CulA-N5A	84.95
		O2A-CulA-NlA	95.06
		O2A-CulA-N2A	177.06
		O2A-Cul A-N3A	93.41
		O2A-Cul A-N5A	95.28
CulB-NIB	2.006	N1B-CulBpN3B	144.92
CulB-N2B	1.974	NlB-CulB-N5B	127.71
CulB-N3B	2.089	N2B-Cul B-NlB	81.94
CulB-N5B	2.236	N2B-Cul B-N3B	86.65
CulB-O2B	1.928	N2B-CulB-N5B	88.76
		N3B-CulB-N5B	84.81
		O2B-CulB-NlB	94.86
		O2B-Cu1B-N2B	174.10
		O2B-CulB-N3B	98.73
		O2B-Cu1B-N5B	89.32
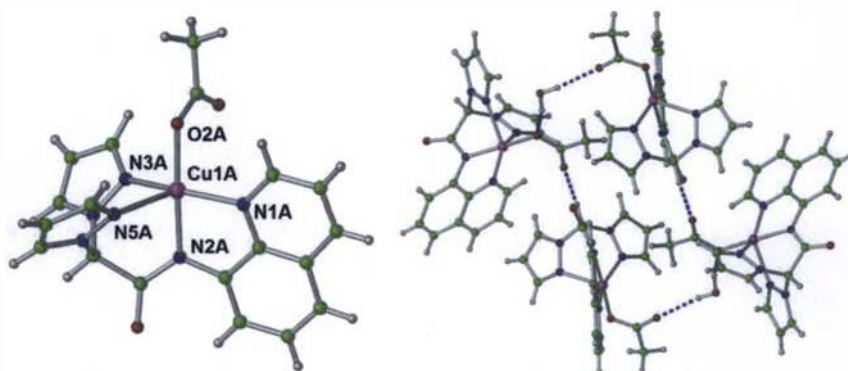
Figure III.16. a) Molecular structure of (L$^\bullet$2Pz)Cu(O$_2$CCH$_3$) (only one independent molecule is shown); b) the intermolecular H-bonding interactions between four (L^{Q}2Pz)Cu(O$_2$CCH$_3$) units and two H$_2$O molecules, forming a [(L^{Q}2Pz)Cu(O$_2$CCH$_3$)]$_4$ tetramer.

Figure III.17. shows the crystal packing of (L^{Q}2pz)Cu(OAc), which propagates due to π-π stacking interactions between the quinoline rings (with a centroid···centroid distance of 3.584 Å, and a perpendicular inter-plane separation of 3.438 Å) , and C-H-π interactions between the quinoline and the pyrazolyl rings of the tetramers (C(3A)-H(3A)···centroid angle of 165.3° and a CH···centroid distance of 3.377 Å).
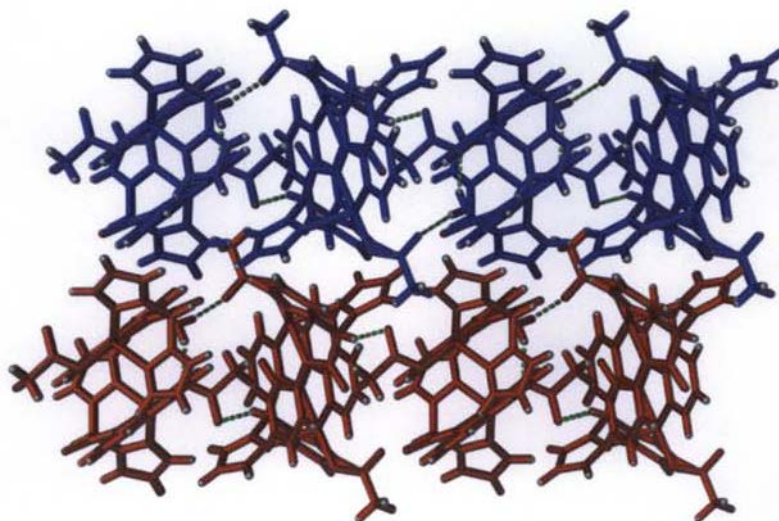
Figure III.17. Crystal packing of (L^{Q}2Pz)Cu(O$_2$CCH$_3$).

III.3. Metalloligands: Design, Syntheses, and Characterization

Having successfully prepared the [(L^{Q}2Pz)Cu(NCCH$_3$)]ClO$_4$ pro-metalloligand, we turned our attention to the synthesis of our desired metalloligands. To achieve our task, instead of sodium acetate we used carboxylic acids having additional coordination sites within their structure.

III.3.1. (L^{Q}2Pz)Cu[O$_2$CCH(pz)$_2$)]

The reaction between [(L^{Q}2Pz)Cu(NCCH$_3$)]ClO$_4$ and bis(pyrazolyl)acetic acid in the presence of one equivalent of potassium hydroxide (to deprotonate the acid) produced, after removal of the KClO$_4$ byproduct, the desired (L^{Q}2Pz)Cu[O$_2$CCH(pz)$_2$)] complex as a green powder. The IR spectrum of the complex (Figure III.18.) clearly proves that amide group maintained its coordination to the copper center,

40

while the UV-Vis spectrum (Figure III.19.) indicates that the square pyramidal geometry around the copper(II) ion is maintained in this complex.

Figure III.18. IR spectrum of HL^Q2Pz (red) and $(L^Q2Pz)Cu[O_2CCH(pz)_2)]$ (blue) highlighting the differences between the free ligand and its copper complex.

Figure III.19. UV-Visible spectrum of $(L^Q2Pz)Cu[O_2CCH(pz)_2)]$

The molecular structure of $(L^Q2Pz)Cu[O_2CCH(pz)_2)]$ is shown at the left of Figure III.20. and selected bond lengths and angles given in Table III.4. X-Ray diffraction experiments revealed that there is one independent molecule per asymmetric unit. In this complex, the copper ion is five-coordinate and bound by one deprotonated nitrogen atom from the amide group, one oxygen atom from the bis(pyrazolyl)acetate ligand, two nitrogen atoms from the two pyrazolyl rings and one nitrogen atom from the quinoline moiety.
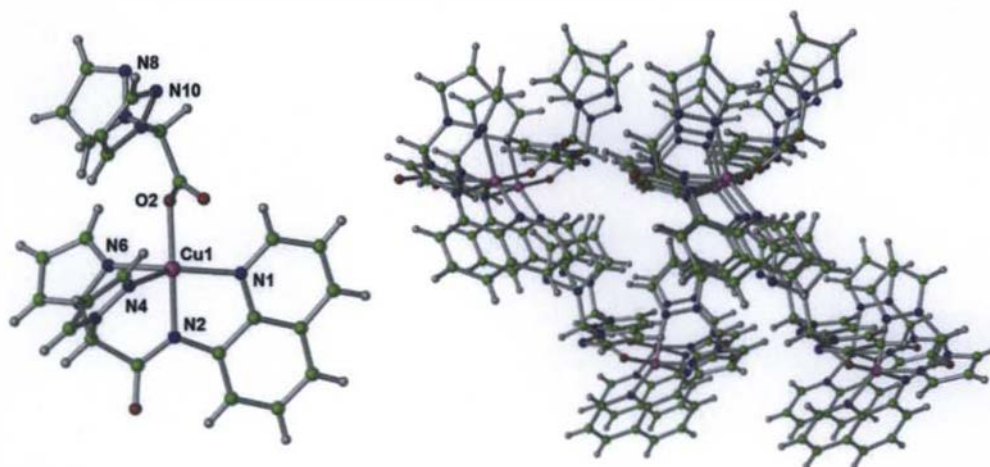
Figure III.20. Structural characteristics of $(L^Q2Pz)Cu[O_2CCH(pz)_2)]$: a) molecular structure and b) crystal packing of the complex.

Table III.4. Selected bond lengths (Å) and angles (°) for $(L^Q2Pz)Cu[O_2CCH(pz)_2)]$.

Atoms	Bond lengths	Atoms	Bond Angles
Cu1-O2	1.944	N1-Cu1-N4	134.60
Cu1-N2	1.974	N1-Cu1-N6	138.12
Cu1-N1	1.994	N2-Cu1-N1	82.44
Cu1-N6	2.126	N2-Cu1-N4	88.07
Cu1-N4	2.151	N2-Cu1-N6	87.82
		N6-Cu1-N4	85.26
		O2-Cu1-N1	97.21
		O2-Cu1-N2	175.19
		O2-Cu1-N4	95.52
		O2-Cu1-N6	89.29

The geometry around the copper(II) center is between trigonal bipyramidal and square pyramidal, with the τ_5 parameter having the value of 0.60. Considering the distorted trigonal bipyramidal geometry, the equatorial plane is formed by the N1, N4 and N6 atoms, while the axial positions are occupied by the N2 and O2 atoms. The distance between Cu1-N2, Cu1-O2 are 1.974 Å and 1.944 Å, respectively. The corresponding N2-Cu1-O2 bond angle is 175.19°. The distance between Cu1-N1, Cu1-N4 and Cu1-N6 are 1.995 Å, 2.151 Å, and 2.126 Å, respectively. The bond angles of N1-Cu1-N4, N1-Cu1-N6 are 134.60° and 138.12°, respectively. The small bite angle (85.26° for N4-Cu1-N6) of the chelating bis(pyrazolyl)methane group is the main factor accounting for this distortion from the ideal trigonal bipyramidal geometry.

The extended structure of $(L^Q2Pz)Cu[O_2CCH(pz)_2)]$ (see Figure III.20.-right) is formed by intermolecular C-H···π interactions (C-H···centroid angle of 108.89° and a C-H···centroid distance of 3.296 Å) involving the quinoline ring (as a H-donor) of one molecule and a pyrazolyl ring (from the bis(pyrazolyl)acetate moiety) of an adjacent molecule. These interactions organize the molecules into a supramolecular polymeric chain which propagate along the a axis of the unit cell. In a separate interaction, the pyrazolyl ring of the ligand of one molecule forms a C-H···π interaction (C-H···centroid angle of 169.08° and a C-H···centroid distance of 3.050 Å) with the pyrazolyl ring of the ligand of the other molecule, while the pyrazolyl ring (from the bis(pyrazolyl)acetate moiety) forms a weak C-H···π interaction (C-H···centroid angle of 140.43° and a C-H···centroid distance of 3.798 Å) with the quinoline ring from other molecule.

The most important structural information gathered from this structure is the fact that the bis(pyrazolyl)acetic acid is coordinated to the copper(II) center *via* the acetate group, leaving the two pyrazolyl rings free for further coordination to a different metallic center.

III.3.2. $(L^Q2Pz)Cu[O_2CCH(CH_2pz)_2)]$

The reaction between $[(L^Q2Pz)Cu(NCCH_3)]ClO_4$ and 1,3-bis(pyrazolyl)-2-butanoic acid in the presence of one equivalent of potassium hydroxide (to deprotonate the acid) produced, after removal of the $KClO_4$ byproduct, the desired $(L^Q2Pz)Cu[O_2CCH(CH_2pz)_2)]$ complex as a green powder. The IR spectrum of the

43

complex (Figure III.21.) clearly proves that amide group maintained its coordination to the copper center, while the UV-Vis spectrum (Figure III.22.) indicates that the square pyramidal geometry around the copper(II) ion is maintained in this complex.
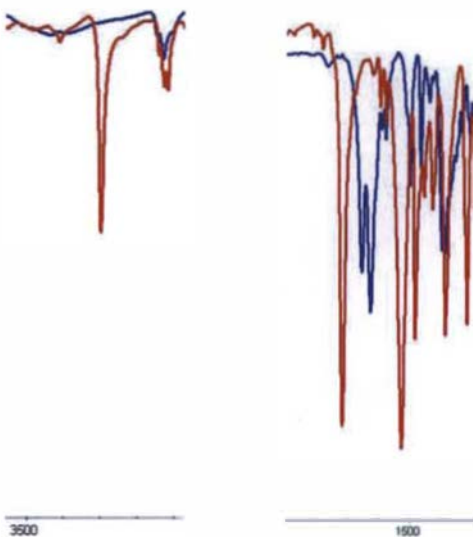

Figure III.21. IR spectrum of HL^Q2Pz (red) and $(L^Q2Pz)Cu[O_2CCH(CH_2pz)_2]$ (blue), highlighting the differences between the free ligand and its copper complex.
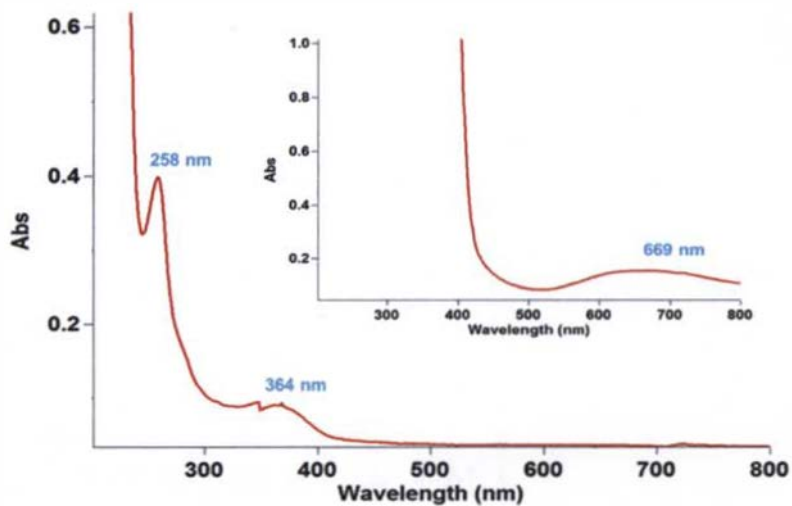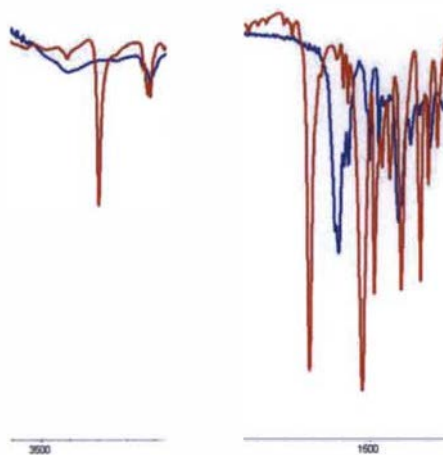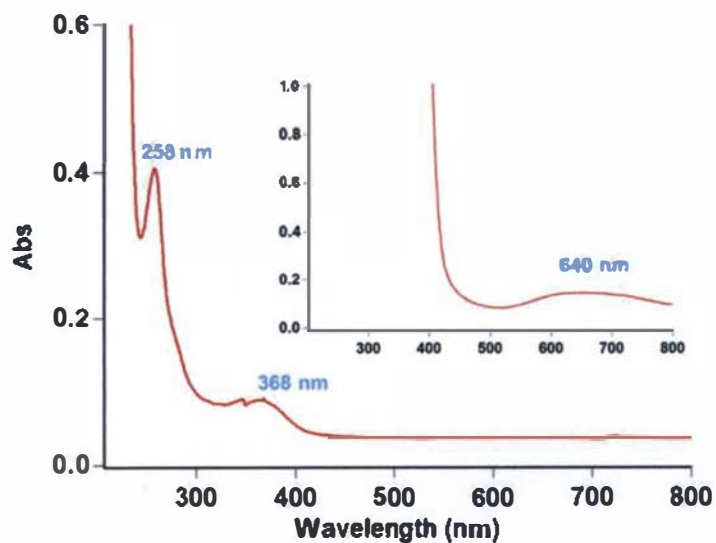

Figure III.22. UV-Visible spectrum of $(L^Q2Pz)Cu[O_2CCH(CH_2pz)_2]$.

X-Ray diffraction experiments were performed on single crystals of this complex; unfortunately, only general features of the structure of this compound can be presented at this time, due to the complexity of the structure of this compound. Figure III.23. shows a representation of the $(L^Q2Pz)Cu[O_2CCH(CH_2pz)_2]$ complex. While detailed structural information cannot be presented at this time, we can say that the copper(II) center is coordinated by a N atom from the quinoline group, a deprotonated amide N atom, two pyrazolyl rings and one oxygen atom from a $O_2CCH(CH_2pz)_2$ moiety. The environment around the Cu^{2+} ion is again between a trigonal bipyramid and a square pyramid; however, information on the τ_5 angle cannot be presented at this time. The same is valid for bond lengths and angles. Regardless of this lack of information on the structural characteristics of this complex, it can be clearly seen that the additional acid is coordinated to the copper(II) center *via* the acetate group, leaving the two pyrazolyl rings free for further coordination to a different metallic center.

Figure III.23. Partially resolved structure of $(L^Q2Pz)Cu[O_2CCH(CH_2pz)_2]$; not yet fully refined, only general structural features are shown.

III.4. Copper(II) – Copper(I) mixed valence complexes

After successfully preparing the desired metalloligands, we have attempted the synthesis of our desired bimetallic derivatives, by reacting the above metalloligands with additional copper centers. The reactions were performed in dichloromethane, by mixing the metalloligands with appropriate metal containing starting materials.

III.4.1. {(L^Q2Pz)Cu^II[O_2CCH(CH_2pz)_2]}_2Cu^I(PF_6)

The reaction of two equivalents of $(L^Q2Pz)Cu[O_2CCH(CH_2pz)_2]$ with one equivalent of $[Cu(NCCH_3)_4]PF_6$ under oxygen free conditions produced a green compound. The IR spectrum of the complex (Figure III.24.) shows that amide group maintained its coordination to the copper(II) center, while the UV-Vis spectrum (Figure III.25.) indicates that the square pyramidal geometry around the same Cu^{2+} ion is maintained in this complex.

Figure III.24. IR spectrum of HL^Q2Pz (red) and $\{(L^Q2Pz)Cu^{II}[O_2CCH(CH_2pz)_2]\}_2Cu^I(PF_6)$ (blue) highlighting the differences between the free ligand and its copper complex.
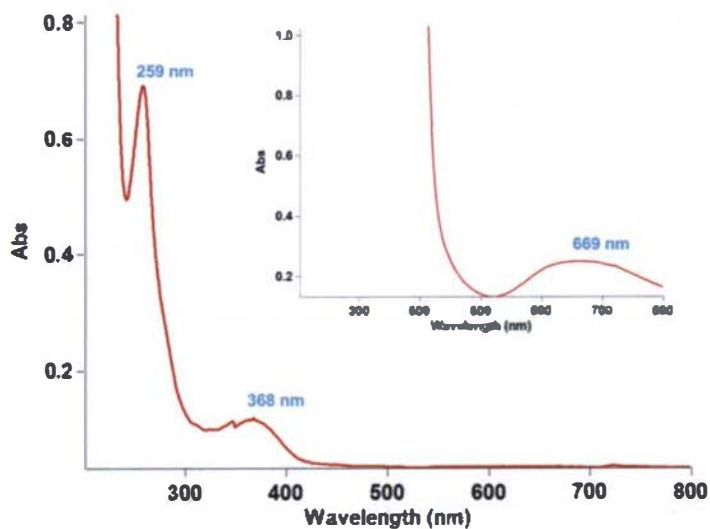
Figure III.25. UV-Visible spectrum of $\{(L^Q2Pz)Cu^{II}[O_2CCH(CH_2pz)_2]\}_2Cu^I(PF_6)$.

X-Ray diffraction experiments were also performed on single crystals of this complex; unfortunately, only the general features of the structure of this compound could be identified, due to the complexity of the structure of this compound. Figure III.26. presents the general structural features of this complex. The copper(II) center is coordinated by a N atom from the quinoline group, a deprotonated amide N atom, two pyrazolyl rings and one oxygen atom from a $O_2CCH(CH_2pz)_2$ moiety. The environment around the Cu^{2+} ion is again between a trigonal bipyramid and a square pyramid; however, information on the τ_5 angle cannot be presented at this time. The same is valid for bond lengths and angles. The 1,3-bis(pyrazolyl)-2-butanoic acid is coordinated to the Cu(II) center *via* its $-COO^-$ moiety and to the Cu(I) center *via* its pyrazolyl rings, thus acting as a bridge between the two metals. The Cu(I) ion is in a distorted tetrahedral geometry; unfortunately, details about bond lengths and angles cannot be presented at this time.
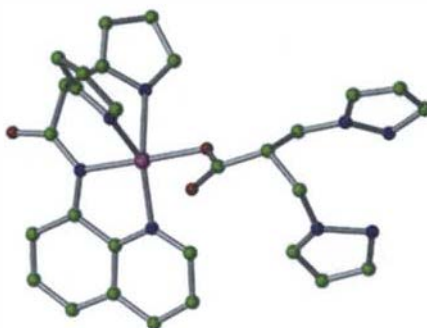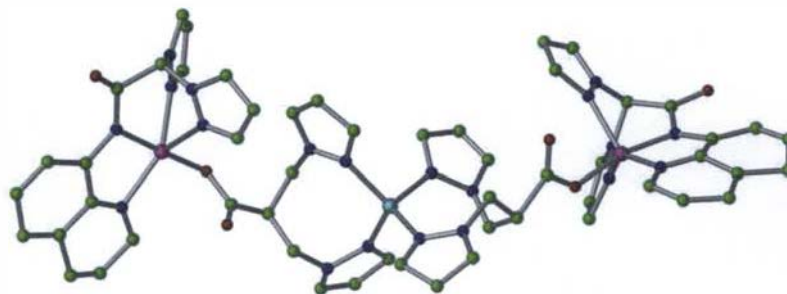

Figure III.26. Partially resolved structure of $\{(L^Q2Pz)Cu^{II}[O_2CCH(CH_2pz)_2]\}_2Cu^I(PF_6)$; not yet fully refined, only general structural features are shown.

III.4.2. $\{(L^Q2Pz)Cu^{II}[O_2CCH(CH_2pz)_2Cu^I(PPh_3)_2]\}NO_3$

The reaction of one equivalent of $(L^Q2Pz)Cu[O_2CCH(CH_2pz)_2]$ with one equivalent of $(Ph_3P)_2CuNO_3$ produced a green compound in good yields. The IR spectrum of the complex (Figure III.27.) shows that amide group maintained its coordination to the copper(II) center, while the UV-Vis spectrum (Figure III.25.) indicates that the square pyramidal geometry around the same Cu^{2+} ion is maintained in this complex.
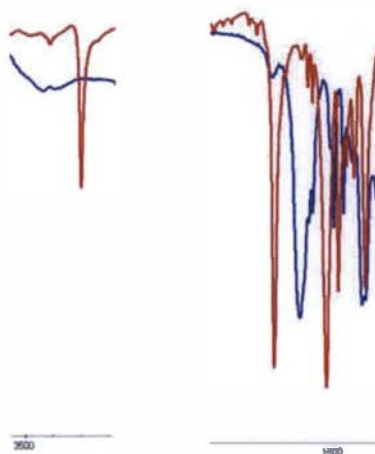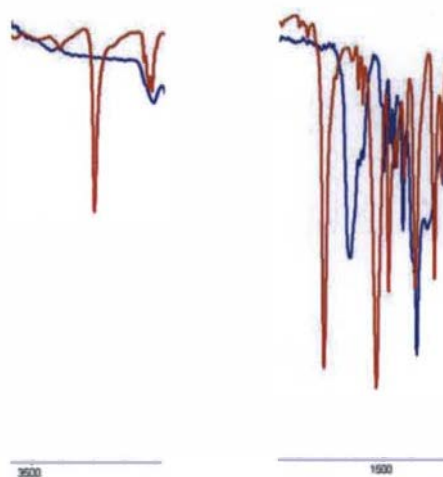
Figure III.27. IR spectrum of $HL^{Q}2Pz$ (red) and $\{(L^{Q}2Pz)Cu^{II}[O_2CCH(CH_2pz)_2Cu^{I}(PPh_3)_2]\}NO_3$ (blue), highlighting the differences between the free ligand and its copper complex.
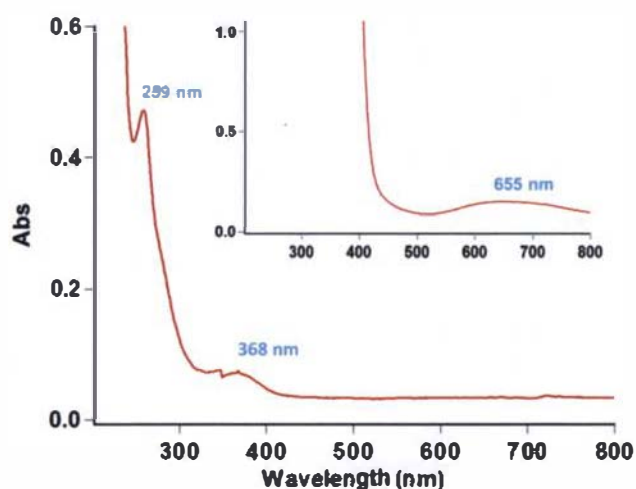
Figure III.28. UV-Visible spectrum of $\{(L^{Q}2Pz)Cu^{II}[O_2CCH(CH_2pz)_2Cu^{I}(PPh_3)_2]\}NO_3$.

The crystal structure of $\{(L^{Q}2Pz)Cu[O_2CCH(CH_2pz)_2Cu(PPh_3)_2]\}NO_3$ is shown in Figure III.29 and selected bond lengths and angles are given in Table III.5. The structure consists of one Cu(II) center originating from the $(L^{Q}2Pz)Cu[O_2CCH(CH_2pz)_2$ metalloligand and one Cu(I) center added additionally. The deprotonated 1,3-bis(pyrazolyl)-2-butanoic acid acts as a bridging ligand between the two copper ions. In this complex, the copper(II) ion (Cu1 in Figure III.29.) is five coordinated and the copper(I) ion (Cu2 in Figure III.29) is four coordinated. The pentacoordinate copper(II) center is coordinated by one deprotonated

48

nitrogen atom from the amide group, one oxygen atom from the acetate ligand, two nitrogen atoms from the two separate pyrazolyl rings and one nitrogen atom from the quinoline moiety. The tetracoordinated Cu(I) center is bound by two nitrogen atoms from the two pyrazolyl rings of the acetate ligand and two phosphorous atoms from the two triphenylphosphine groups.

The geometry around Cu1 is in between trigonal bipyramidal and square pyramidal, with the τ_5 parameter having the value of 0.47. Considering the distorted square pyramidal geometry, the square plane is defined by the N1, N2, N4 and O2 atoms, with the N6 atom occupying the apical position. The distance between Cu1-N1, Cu1-N2, Cu1-N4 and Cu1-O2 are 2.020 Å, 1.988 Å, 2.133 Å and 1.937 Å, respectively. The distance between Cu1-N6 is 2.172 Å. The bond angles of N1-Cu1-N2, N2-Cu1-N4, N4-Cu1-O2 and N1-Cu1-O2 are 81.93°, 89.30°, 89.75° and 93.17°, respectively. The geometry around Cu2 is best described as distorted tetrahedral, which is due to the presence of the bulky triphenylphosphine groups (the P1-Cu2-P2 bond angle is 122.25°), and the bite angle of the two pyrazolyl rings of the bridging ligand. The distance between Cu2-N8, Cu2-N10, Cu2-P1 and Cu2-P2 are 2.094 Å, 2.083 Å, 2.3186 Å and 2.3035 Å, respectively. The distance between the two copper centers is 7.452 Å.

Table III.5. Selected bond lengths (Å) and angles (°) for {(L^{Q}2Pz)Cu^{II}[O$_2$CCH(CH$_2$pz)$_2$Cu^I(PPh$_3$)$_2$]}NO$_3$.

Atoms	Bond lengths	Atoms	Bond Angles
Cu1-N1	2.020	N1-Cu1-N4	142.49
Cu1-N2	1.988	N1-Cu1-N6	130.75
Cu1-N4	2.133	N2-Cu1-N1	81.93
Cu1-N6	2.172	N2-Cu1-N4	89.30
Cu1-O2	1.937	N2-Cu1-N6	86.15
		N4-Cu1-N6	84.46
		O2-Cu1-N1	93.17
		O2-Cu1-N2	170.57
		O2-Cu1-N4	89.75
		O2-Cu1-N6	103.10
Cu2-N8	2.094	N8-Cu2-P1	107.05
Cu2-N10	2.083	N8-Cu2-P2	105.39
Cu2-P1	2.3186	N10-Cu2-N8	110.39
Cu2-P2	2.3035	N10-Cu2-P1	102.88
		N10-Cu2-P2	108.68
		P2-Cu2-P1	122.25
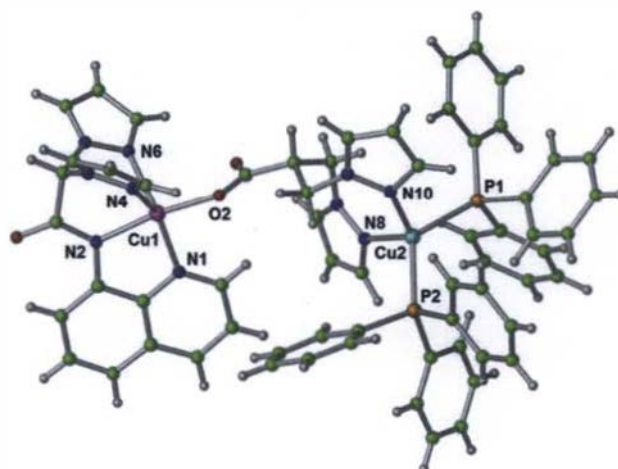
Figure III.29. Molecular structure of the $\{(L^Q2Pz)Cu^{II}[O_2CCH(CH_2pz)_2Cu^I(PPh_3)_2]\}^+$ cation.

References

1. Semeniuc, R. F.; Reamer, T. J.; Smith, M. D. *New J. Chem.*, **2010**, *34*, 439-452.

2. Semeniuc, R. F.; Reger, D. L. *Eur. J. Inorg. Chem.* **2016**, 2253.

3. Pettinari, C.; Pettinari R. *Coord. Chem. Rev.* **2005**, *249*, 663.

4. Bioinformatics in Tropical Disease Research: A Practical and Case-Study Approach [Internet], https://www.ncbi.nlm.nih.gov/books/NBK6824/ (accessed on 10.22.2017)

5. Collins, T. J. *Acc. Chem. Res.* **1994**, *27*, 279.

6. Lucas, R.; Zart, M.K.; Mukherjee, J.; Sorrell, T. N.; Powell, D. R.; Borovik, A.S. *J. Am. Chem. Soc.* **2006**, *128*, 15476.

7. https://en.wikipedia.org/wiki/Geometry_index (accessed on 11.20.2017)

IV. Conclusions and Future Work

The research discussed in this study focused on the design, synthesis, and characterization of new complexes that have the potential to mimic the structure and function of various active centers found in several enzymes. In the work presented here, a multi-step synthetic process was used to create a new ligand that consists of a quinoline body, an amido group linkage, and a bis(pyrazolyl)methane donor set.

This ligand was then coordinated to a copper(II) center, to form a pro-metalloligand, consisting in the deprotonated ligand surrounding a Cu(II) ion; in addition, the metallic center was fitted with a labile group (*i.e.* acetonitrile), easily replaced by other organic moieties with donor properties. Specifically, two carboxylic acids (*i.e.* bis(pyrazolyl)acetic acid and 1,3-bis(pyrazolyl)-2-butanoic acid) were used to prepare the desired metalloligands by replacing the labile group, through a charge assisted metathesis process.

These metalloligands were then used to prepare mixed valence Cu(II)/Cu(I) metal complexes; all these compounds were studied and characterized by IR and UV-Vis spectroscopies, and X-ray crystallography.

IR spectroscopy showed that the ligand coordinated to the copper(II) center *via* its deprotonated amido group. UV-Vis spectroscopy demonstrated that the copper(II) center is found in a square pyramidal geometry in all cases, regardless of the fifth ligand attached to the metallic center. This means that, in addition to the deprotonated amido group, the copper center is surrounded by the remaining nitrogen atoms of the ligand, as well as an additional solvent molecule.

X-Ray crystallographic investigations confirmed the above structure of all prepared complexes. In all compounds, the environment around each of the copper(II) ions consists in a geometry between a square pyramid and a trigonal bipyramid, as shown by the copper ion's τ_5 value, around 0.5.

The reaction of Cu(I) ions with the prepared metalloligands afforded Cu(II) / Cu(I) mixed valence complexes, which were also characterized by IR and UV-Vis spectroscopies, and X-ray crystallography. These complexes maintain the original coordination around the copper(II) center, the structural differences being practically negligible. In contrast to the Cu(II) ions, the Cu(I) species are found in a

distorted tetrahedral environment, as expected, and surrounded by the second donor site of the preformed metalloligands.

Future work would include the investigation the catalytic properties of these complexes in oxidation reactions. Of interest would be the oxidation of catechols to their corresponding quinones, or of ortho-aminophenols to phenoxazinones. If the Cu(II) complex would have a nitrite group as the secondary ligand, other studies could be focused on the nitrite reductase properties of these compounds.

In addition, the bis(pyrazolyl)acetic acid could be replaced by other acids having attached a second donor set, to study the influence of a different coordination group on the properties of the resulting complexes. This would give more insight if the bridge between the two copper centers is an important factor in catalytic activity. If the activity increases, it would indicate that a certain type and/or size of a bridge would be needed in order to observe the desired catalytic activities.

Appendices

Appendix A

Contents

Appendix B

Contents

Table S1. Crystal data and structure refinement details for $(L^Q2Pz)Cu(BF_4)$.

Chemical formula	$C_{17}H_{13}BCuF_4N_6O$
M_r	467.68
Crystal system, space group	Monoclinic, $P2_1/n$
Temperature (K)	100
a, b, c (Å)	9.1850 (4), 17.3019 (6), 12.1405 (4)
β (°)	90.977 (2)
V (Å^3)	1929.06 (12)
Z	4
Radiation type	Cu $K\alpha$
μ (mm^{-1})	2.15
Crystal size (mm)	$0.17 \times 0.16 \times 0.08$
Absorption correction	Multi-scan, *SADABS2014*/7, Bruker AXS
T_{min}, T_{max}	0.671, 0.753
No. of measured, independent and observed [$I > 2\sigma(I)$] reflections	28188, 3488, 2940
R_{int}	0.052
$(\sin \theta/\lambda)_{max}$ (Å^{-1})	0.602
$R[F^2 > 2\sigma(F^2)], wR(F^2), S$	0.045, 0.167, 1.06
No. of reflections	3488
No. of parameters	271
H-atom treatment	H-atom parameters constrained
$\Delta\rho_{max}, \Delta\rho_{min}$ (e Å^{-3})	0.96, − 0.81

Table S2. Crystal data and structure refinement details for [(L^{Q}2Pz)Cu(NCCH$_3$)]ClO$_4$.

Chemical formula	C$_{19}$H$_{16}$CuN$_7$O·ClO$_4$
M_r	521.38
Crystal system, space group	Monoclinic, $C2/c$
Temperature (K)	100
a, b, c (Å)	29.990 (3), 8.1215 (8), 17.9630 (16)
β (°)	104.213 (4)
V (Å^3)	4241.2 (7)
Z	8
Radiation type	Cu $K\alpha$
μ (mm^{-1})	3.05
Crystal size (mm)	0.28 × 0.17 × 0.13
Absorption correction	Multi-scan, $SADABS2014$/7, Bruker AXS
T_{min}, T_{max}	0.591, 0.753
No. of measured, independent and observed [$I > 2\sigma(I)$] reflections	45384, 3891, 3683
R_{int}	0.051
$(\sin \theta/\lambda)_{max}$ (Å^{-1})	0.602
$R[F^2 > 2\sigma(F^2)]$, $wR(F^2)$, S	0.033, 0.085, 1.06
No. of reflections	3891
No. of parameters	309
No. of restraints	36
H-atom treatment	H-atom parameters constrained
$\Delta\rho_{max}, \Delta\rho_{min}$ (e Å^{-3})	0.66, −0.53

Table S3. Crystal data and structure refinement details for $(L^Q2Pz)Cu(OAc)$.

Chemical formula	$C_{38}H_{32.58}Cu_2N_{12}O_{6.29}$
M_r	885.06
Crystal system, space group	Triclinic, P
Temperature (K)	100
a, b, c (Å)	9.6542 (6), 13.8554 (8), 16.0283 (9)
α, β, γ (°)	114.194 (3), 93.294 (3), 103.183 (3)
V (Å^3)	1876.4 (2)
Z	2
Radiation type	Cu $K\alpha$
μ (mm^{-1})	1.96
Crystal size (mm)	$0.29 \times 0.12 \times 0.11$
Absorption correction	Multi-scan, *SADABS 2014*/7, Bruker AXS
T_{min}, T_{max}	0.615, 0.753
No. of measured, independent and observed $[I > 2\sigma(I)]$ reflections	42487, 6729, 6034
R_{int}	0.04
$(\sin \theta/\lambda)_{max}$ (Å^{-1})	0.602
$R[F^2 > 2\sigma(F^2)]$, $wR(F^2)$, S	0.041, 0.121, 1.08
No. of reflections	6729
No. of parameters	538
No. of restraints	6
$\Delta\rho_{max}, \Delta\rho_{min}$ (e Å^{-3})	0.85, −0.47

Table S4. Crystal data and structure refinement details for $(L^Q2Pz)Cu[O_2CCH(pz)_2)]$.

Chemical formula	$C_{25}H_{20}CuN_{10}O_3$
M_r	572.05
Crystal system, space group	Monoclinic, $P2_1$
Temperature (K)	100
a, b, c (Å)	8.8848 (3), 15.2219 (5), 9.6991 (4)
β (°)	112.056 (2)
V (Å^3)	1215.74 (8)
Z	2
Radiation type	Cu $K\alpha$
μ (mm^{-1})	1.71
Crystal size (mm)	$0.43 \times 0.41 \times 0.07$
Absorption correction	Multi-scan, *SADABS2014*/7, Bruker AXS
T_{min}, T_{max}	0.591, 0.753
No. of measured, independent and observed $[I > 2\sigma(I)]$ reflections	14078, 4255, 4197
R_{int}	0.034
$(\sin \theta/\lambda)_{max}$ (Å^{-1})	0.602
$R[F^2 > 2\sigma(F^2)]$, $wR(F^2)$, S	0.027, 0.069, 1.05
No. of reflections	4255
No. of parameters	352
No. of restraints	1
$\Delta\rho_{max}, \Delta\rho_{min}$ (e Å^{-3})	0.39, −0.20

Table S5. Crystal data and structure refinement details for $\{(L^Q2Pz)Cu^{II}[O_2CCH(CH_2pz)_2Cu^I(PPh_3)_2]\}NO_3$.

Chemical formula	$C_{61}H_{54}Cu_2N_{11}O_6P_2 \cdot 3(CH_2Cl_2)$
M_r	1521.03
Crystal system, space group	Triclinic, P
Temperature (K)	100
a, b, c (Å)	13.4052 (7), 14.3404 (7), 19.2792 (9)
α, β, γ (°)	77.040 (3), 70.484 (3), 81.514 (3)
V (Å^3)	3393.6 (3)
Z	2
Radiation type	Cu $K\alpha$
μ (mm^{-1})	2.4
Crystal size (mm)	$0.49 \times 0.20 \times 0.11$
Absorption correction	Multi_scan, $SADABS2014/7$, Bruker AXS
T_{min}, T_{max}	0.499, 0.753
No. of measured, independent and observed $[I > 2\sigma(I)]$ reflections	74031, 12100, 10174
R_{int}	0.056
$(\sin \theta/\lambda)_{max}$ (Å^{-1})	0.602
$R[F^2 > 2\sigma(F^2)]$, $wR(F^2)$, S	0.045, 0.172, 1.14
No. of reflections	12100
No. of parameters	794
$\Delta\rho_{max}, \Delta\rho_{min}$ (e Å^{-3})	1.10, −0.58

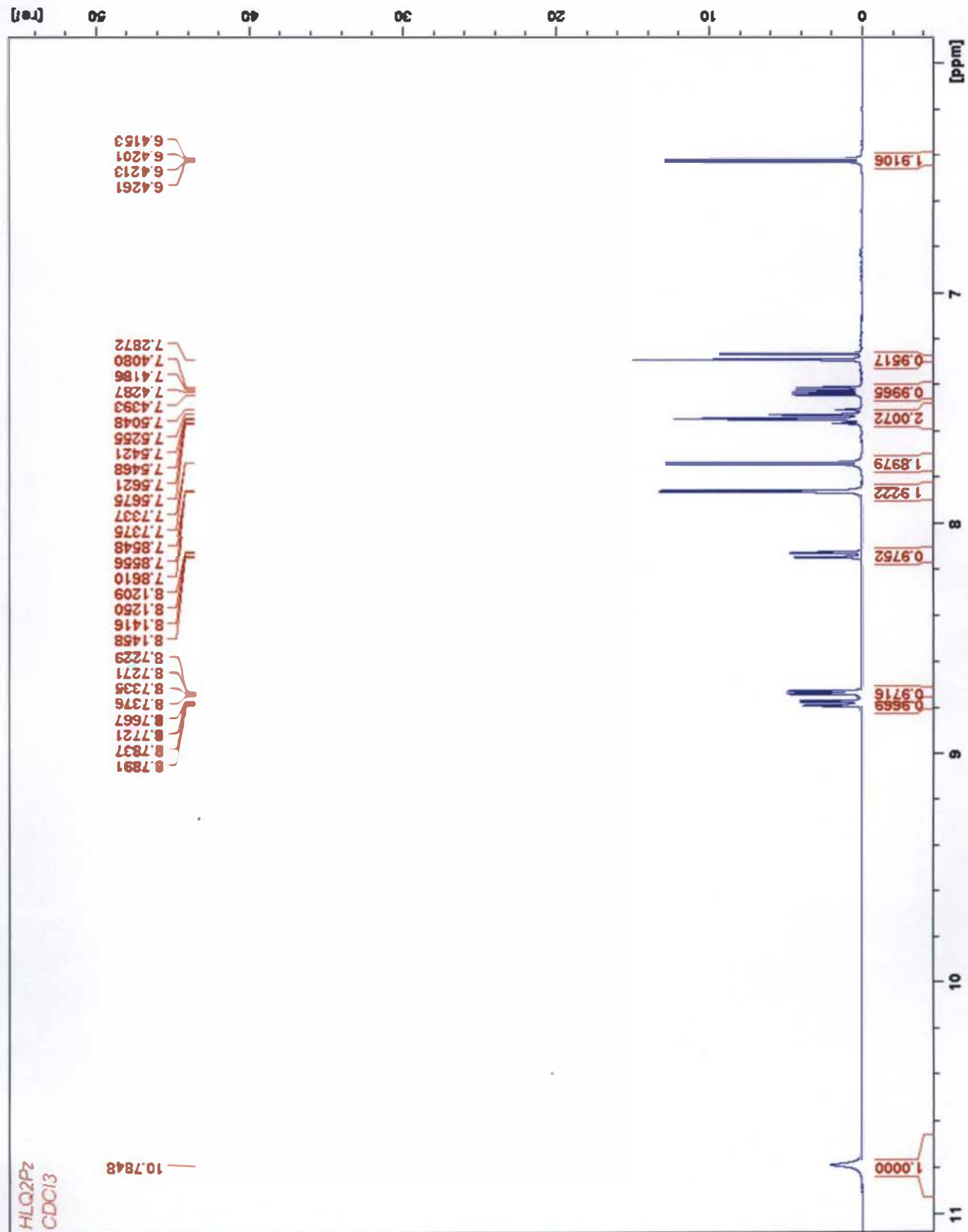**Figure S1.** NMR spectrum of the HL^{Q}2Pz ligand.

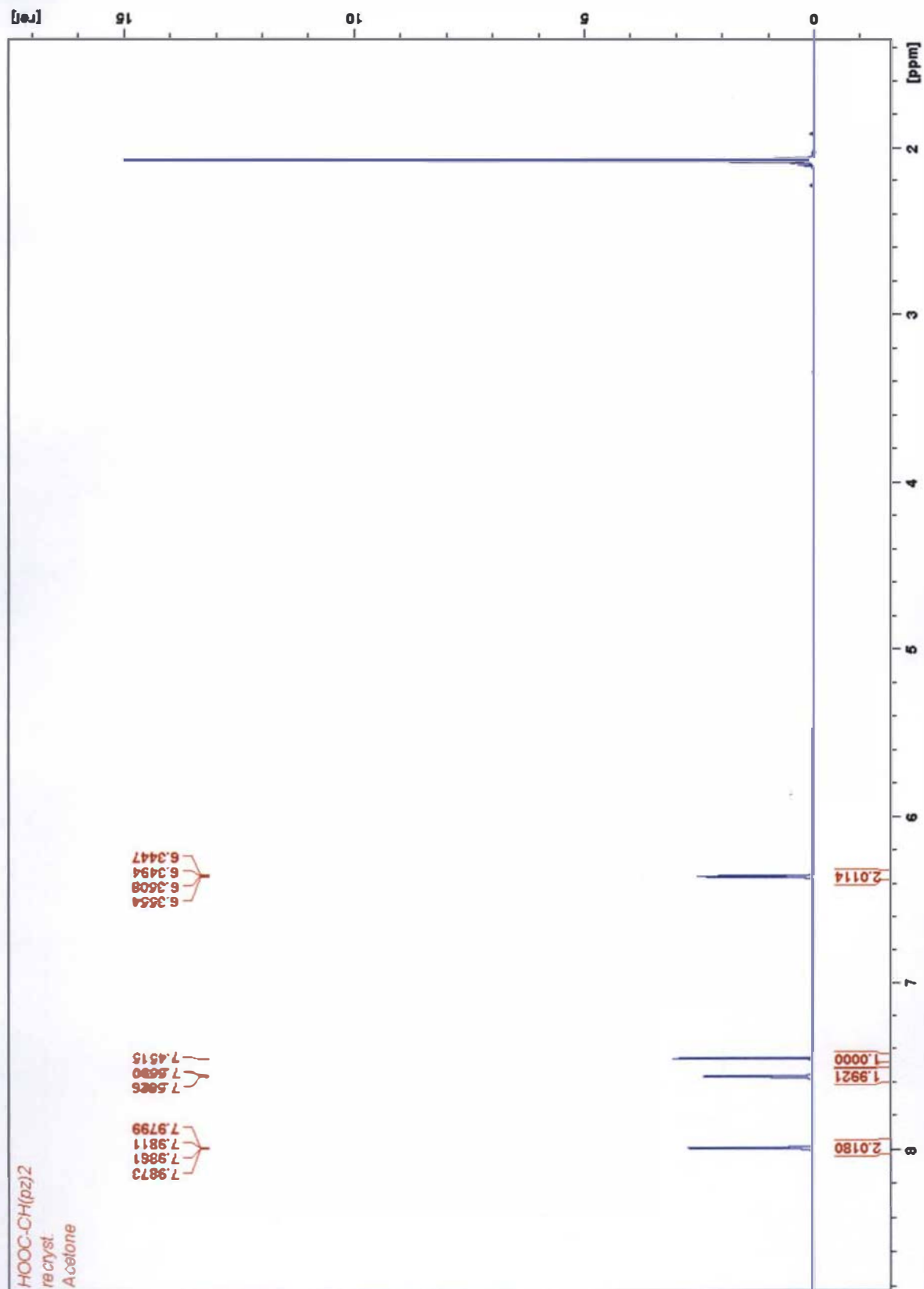**Figure S2.** NMR spectrum of the bis(pyrazolyl)methane acetic acid.

Figure S3. NMR spectrum of the 2-methylpyrazolyl-3-pyrazolyl propanoic acid.